Mesoscale Convective System Development, Synoptic Drivers, and Forecast Challenges of a Catastrophic Coastal Rainfall Event in West Africa

IBRAHIM TOURÉ SALIFOU,[a] MARLON MARANAN,[b] ANDREAS H. FINK,[b] KOUAKOU KOUADIO,[a,d] FIDÈLE YOROBA,[a,d] N'DATCHOH E. TOURÉ,[a] TOKA ARSÈNE KOBEA,[a] AND A. DIEDHIOU[a,c]

[a] *Laboratoire des Sciences de la Matière, de l'Environnement et de l'énergie Solaire, Université Félix Houphouët-Boigny, Abidjan, Côte d'Ivoire*
[b] *Karlsruhe Institute of Technology, Karlsruhe, Germany*
[c] *Institute of Environmental Geosciences, Université Grenoble Alpes, IRD, CNRS, Grenoble INP, Grenoble, France*
[d] *Station Géophysique de Lamto, N'Douci, Côte d'Ivoire*

(Manuscript received 1 February 2025, in final form 24 September 2025, accepted 20 October 2025)

ABSTRACT: This study elaborates on the (thermo)dynamical drivers of the second highest daily rainfall amount in historical records in the largest Ivorian city Abidjan with over 300 mm, which occurred on 18–19 June 2018 and caused severe socioeconomic damages in this metropolis. Based on unique (sub)daily rainfall data from stations across the District of Abidjan, this extreme amount was highly localized but embedded in a widespread area of daily totals in excess of 100 mm. Leveraging infrared and microwave satellite imagery, ERA5 reanalysis, as well as European Centre for Medium-Range Weather Forecasts deterministic and ensemble predictions, the following results are obtained. First, the extreme event was associated with a westward-propagating, long-lasting coastal mesoscale convective system (MCS), which, remarkably, was in a weakening stage as it entered the District of Abidjan. Then, a moist low-tropospheric vortex developed when the MCSs approached Abidjan. It was generated via vorticity tilting and vortex stretching most likely through interaction with the MCS, causing exceptionally high values of both moisture flux convergence and precipitable water. Finally, according to the extreme forecast index patterns in successive forecasts, an extreme event over the District of Abidjan was not predicted until roughly 12 h before rainfall onset, highlighting considerable challenges in the forecasting of this case. This study emphasizes the need to improve the representation of MCS–vortex interactions in numerical weather prediction models as a means to enhance early warning systems and climate services for extreme flood-inducing precipitation events in West African cities.

KEYWORDS: Convergence/divergence; Climate change; Convective storms; Mesoscale processes; Mesoscale systems; Operational forecasting

1. Introduction

Extreme rainfall events and their associated impacts, including flash floods and landslides, have been recognized as among the most catastrophic natural disasters globally and have considerably affected cities across West Africa in the last few decades (Douglas et al. 2008). Some works conducted across West African conurbations such as Abidjan in Côte d'Ivoire (Konate et al. 2016; Amouin et al. 2021; Coulibaly et al. 2024), Accra in Ghana (Atiah et al. 2023), Dakar in Senegal (Engel et al. 2017; Diedhiou et al. 2024), Lagos in Nigeria (Abiodun et al. 2017), and Ouagadougou in Burkina Faso (Engel et al. 2017; Lafore et al. 2017) showcased the severity of flood-causing rainfall with significant repercussions on populations, goods, infrastructures, and socioeconomic activities. Such events, paired with their projected intensification due to global warming (IPCC 2022), rapid population growth in particular in the densely urbanized coastal region, and ongoing improper city planning such as unsuitable drainage systems (Douglas et al. 2008), stress the urgent need for effective disaster risk management and early warning systems, for which an improved understanding of the nature of extreme West African rainfall is key.

Rainfall patterns in West Africa are predominantly controlled by the West African monsoon system, which is characterized by spatial and temporal variability across the region from multidecadal down to synoptic time scales (e.g., Sultan et al. 2003; Fink et al. 2006; Nicholson 2013; Nicholson et al. 2018). On subseasonal to daily time scales, rainfall extremes in West Africa have experienced a significant increase in frequency over the last decades (Panthou et al. 2014; Sanogo et al. 2015; Nkrumah et al. 2019; Vischel et al. 2019) and are expected to intensify under climate change according to the Clausius–Clapeyron (CC) scaling (Fitzpatrick et al. 2020), at subdaily time scales even higher than CC scaling (Kendon et al. 2019). Accordingly, the body of studies related to extreme rainfall events has increased to improve the understanding of the physical processes and environmental conditions around intense rainfall systems. There is general consensus on the southwesterly inflow of moisture (Thorncroft et al. 2011; Vizy and Cook 2018, 2022) and midlevel disturbances in the form of

Denotes content that is immediately available upon publication as open access.

Supplemental information related to this paper is available at the Journals Online website: https://doi.org/10.1175/MWR-D-25-0021.s1.

Corresponding author: Ibrahim Touré Salifou, salifoutoure.ibrahim@gmail.com

DOI: 10.1175/MWR-D-25-0021.1

African easterly waves (AEWs; Burpee 1972; Reed et al. 1977; Fink and Reiner 2003; Berry and Thorncroft 2005; Janiga and Thorncroft 2016; Tomassini et al. 2017) acting as facilitators for the development and sustainment of life cycles of organized mesoscale convective systems (MCSs). AEWs alter the midlevel flow and are thus capable of controlling the low-level wind shear field (Mohr and Thorncroft 2006), which has intensified over the past decades arguably due to the effect of Saharan warming (Taylor et al. 2017), as well as midtropospheric dryness (Rowell and Milford 1993), which can give rise to damaging squall lines (Fink and Reiner 2003). While squall lines are a prominent phenomenon over the Sahel (Peters and Tetzlaff 1988; Mathon and Laurent 2001; Redelsperger et al. 2002; Mathon et al. 2002; Fink and Reiner 2003; Bickle et al. 2021), rainfall systems over the moister Guinea Coast are more diverse, ranging from weak shallow convection to mature MCSs with pronounced convective cores (Maranan et al. 2018). Nonetheless, while of smaller relative importance compared to the Sahel, MCS-type features overall still account for more than half of total annual rainfall at the Guinea Coast (Maranan et al. 2018).

In recent times, case studies on West African rainfall extremes emphasized the slow-moving or decelerating nature of the relevant MCSs as an important element to extreme rainfall accumulations. The infamous Sahelian Ouagadougou event on 1 September 2009 included the stalling of an MCSs, caused by the breaking of a record-breaking strong AEW (Cornforth et al. 2017; Engel et al. 2017; Lafore et al. 2017; Beucher et al. 2020). Maranan et al. (2019) investigated the life cycle of a long-lived MCS that caused intense rainfall amounts in Nigeria and along the Guinea Coast after having transitioned from a rapidly moving squall line to a slow coastal system. Both cases involved the development of a lower-tropospheric vortex and strong convergent motions, through which extreme moisture levels were reached.

However, the way the respective vortices interacted with convective systems varied between these two cases. While the associated vortex facilitated a moisture refueling in the wake of the primary MCS and thus the formation of a secondary convective cell in the Ouagadougou event, it preconditioned the study area in the Nigerian case with abundant moisture, triggering an explosive intensification of the MCS upon its arrival. This marked the transition of the MCS from a fast Sahelian squall line to a slower-moving organized convective system. The latter also appeared to be related to the formation of a vortex which was an accompanying characteristic feature of the long-lived convective systems that moved westward along the Guinea Coast region.

In general, the relevance of such low–midlevel vortices for rainfall over the Guinea Coast region is documented (Knippertz et al. 2017; Vondou et al. 2026), which can trigger prolonged rainy episodes even in the absence of AEWs (Fink et al. 2006). However, due to the small number of studies, there is a limited understanding of the interactions between the vortices and MCSs in the moist coastal regime and how rainfall extremes can subsequently be triggered. For the drier Sahel and Soudan regions, the works of Tomassini et al. (2017) and Beucher et al. (2020) provide potential coupling frameworks associated with moist convection and AEW-related vortices. While the latter study emphasizes the existence of a large-scale wet spell to create an oceanic-type environmental setting that prevents strong subcloud evaporation of rainfall, both highlight moisture convergence and vortex stretching according to the vorticity tendency equation as key elements for the development of extreme rainfall within a convection–AEW interaction. Although abundant moisture is prevalent in the Guinea Coast region already, it is not known whether similar considerations of these convection–vortex interactions can be transferred to this region.

Furthermore, an often-overlooked aspect to extreme events is rainfall produced by systems with weaker (i.e., shallower) convective signatures than the archetypical deep Sahelian MCSs. Through the evaluation of vertical radar echo profiles, Hamada et al. (2015) related strongest rainfall to precipitation systems with bottom-heavy echoes, indicative of dominant warm-rain processes, in regimes with abundant low-level moisture. These findings, derived from satellite-borne radar over pantropical regions, are confirmed by Xu et al. (2022), who further placed frequent occurrences of such systems over coastal monsoon regions.

To increase the body of knowledge with respect to intense West African coastal rainfall and their dynamical evolution, this study investigates the MCS and environmental characteristics of an extreme case which caused more than 300 mm within less than a day on 18–19 June 2018 in the District of Abidjan (Côte d'Ivoire). This event led to 20 deaths, extensive urban floodings, and estimated economic losses of nearly 29 million U.S. dollars [Post Disaster Needs Assessment (PDNA) 2019; Coulibaly et al. 2024]. In advance of findings presented later in this manuscript, this case serves as a cautionary example of a rather inconspicuously shallow but eventually flood-inducing MCS, the rainfall output of which only came to light by leveraging a unique set of in situ rainfall data. Because of the magnitude of this event, part of this study is dedicated to its practical predictability in a state-of-the-art global model. It is relevant insofar as the forecasting of daily rainfall over West Africa, and such extremes in particular, is notoriously difficult for current numerical weather models (Haiden et al. 2012; Vogel et al. 2018, 2020) but at the same time vital for early warnings of flood risk (e.g., Ward et al. 2020; Kreibich et al. 2022).

The manuscript is structured as follows: Section 2 describes the data and methods employed. Then, section 3 presents results and discussion on the evolution of the extreme rainfall event, the involved convective and dynamical features, and the forecast challenges at lead times up to 5 days. Finally, section 4 provides a summary and conclusions.

2. Data and methods

a. Study area

The study area mainly covers the southern part of West Africa (Fig. 1a), with a particular focus on the District of Abidjan (Fig. 1b), the economic capital of Côte d'Ivoire, which has an estimated population of over six million inhabitants, accounting for

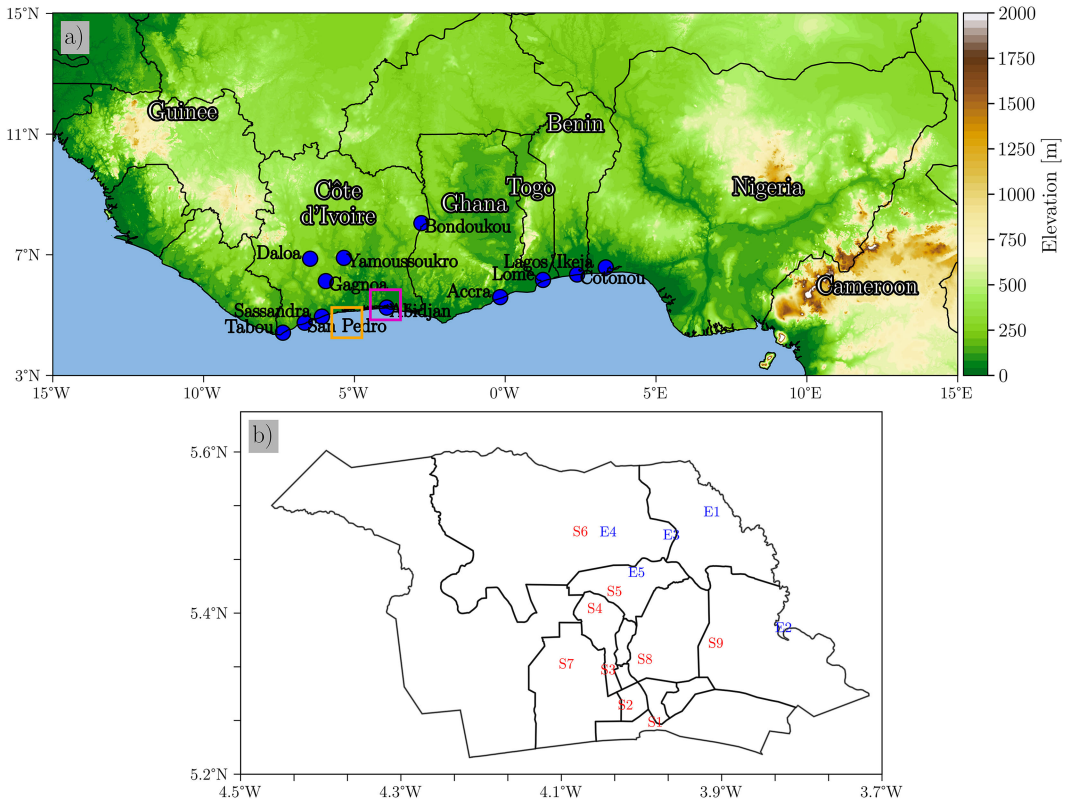

FIG. 1. (a) Topography of WA (m) based on the Global Land One-kilometer Base Elevation (GLOBE) digital elevation model (Hastings et al. 2000), and blue dots represent KASS-D stations. The purple and orange boxes at the coast of Côte d'Ivoire indicate focus domains that are used in the analysis of the (thermo)dynamical controls in section 3c onward. We refer to the text therein for more details. (b) District of Abidjan and station names. The letters S and E represent the SODEXAM and EVIDENCE stations, respectively.

21.5% of the total Ivorian population (Recensement Général de la Population et de l'Habitat 2022). The climate of West Africa is controlled by the West African monsoon. The Guinea Coast region has a bimodal rainy season peaking in June and October with a little dry season in between and the major dry season from November to February (Fink et al. 2017). The District of Abidjan exhibits a similar bimodal pattern as West Africa (WA). Based on long-term rainfall records dating back to 1936 at the Abidjan station from the Karlsruhe African Surface Station-Database (KASS-D; Vogel et al. 2018), the annual-mean precipitation is about 1832 mm, while the mean precipitation in the month of June reaches 526 mm.

b. *Reanalysis and (ensemble) forecast datasets*

The atmospheric variables used in this study are taken from the ERA5 reanalysis (Hersbach et al. 2020), produced by the European Centre for Medium-Range Weather Forecasts (ECMWF), with a spatial resolution of ~31 km and hourly temporal resolution. Data were extracted hourly from June 1991 to June 2020 to define a 30-yr reference period. The variables used are vertical (W) and horizontal (U and V) winds, total precipitation (TP), precipitable water (PW), relative vorticity, and vertically integrated moisture flux (VIMF) and vertically integrated moisture divergence (VIMD). Negative VIMD values are termed moisture flux convergence (MFC) hereafter. Low-tropospheric flow was estimated using a mass-weighted average of horizontal winds between 600 and 950 hPa (Lafore et al. 2017; Maranan et al. 2019). These two pressure levels are also used to determine the low-level wind shear (LLWS) expressed as the wind vector difference between these layers, a common proxy for studying prestorm conditions in West Africa (e.g., Klein and Taylor 2020; Baidu et al. 2022). We note that ERA5 rainfall does not represent assimilated rainfall observations but stems from ECMWF short-range forecast and, thus, relies on convection parameterization. Despite the known challenges of ERA5 to reliably capture rainfall in tropical regions (Lavers et al. 2022), ERA5 rainfall is used in this study in a supportive role for the analysis of environmental settings around the area of extreme precipitation.

This study also uses operational, high-resolution (HRES) deterministic and ensemble (ENS) forecasts. At a native spatial grid spacing of roughly 9 km each, they are produced by the Integrated Forecasting System (IFS; cycle 46r1 in June 2019) which features a moist convection parameterization scheme based on Bechtold et al. (2014). These forecasts, retrieved with a spatial resolution of 0.25° to match that of ERA5, are initialized at 1200 UTC with an integration period of up to 10 and 15 days, respectively. Given the typical skill

decline beyond day 6 (Haiden et al. 2012; Pantillon et al. 2017; Vogel et al. 2018), only lead times of 1–5 days were considered. From the ECMWF Ensemble Prediction System (EPS), the extreme forecast index (EFI) and the shift of tails (SOT) are taken, both of which are explained in further detail in section 2f.

c. Station and gridded rainfall data

The present work utilizes rain gauge data from various sources. Regarding the District of Abidjan, daily (0800–0800 UTC) precipitation is provided by "Société d'Exploitation et de Développement Aéroportuaire, Aéronautique et Météorologique (SODEXAM)." Additionally, hourly rain gauge (RG) data across five stations from the "Evènements pluvieux extrêmes, vulnérabilités et risques Environnementaux: inondation et Contamination des Eaux (EVIdENCE; EVIDENCE)" project (Zahiri et al. 2023) were acquired (see Table S1 in the online supplemental material). Both have been made available from 17 to 20 June 2018 (Fig. 1b), covering the period before, during, and after the extreme rainfall event. An extended, climatological view of rainfall along the Guinea Coast is provided from the KASS-D in Fig. 1a (Vogel et al. 2018). Regional-scale rainfall is analyzed with the Integrated Multi-SatellitE Retrievals for Global Precipitation Measurement (GPM) (IMERG) version 7 dataset (Huffman et al. 2023). IMERG is a gridded level-3 rainfall product that provides rainfall estimates every 30 min at a spatial resolution of 0.1° × 0.1°. Its algorithm is based on the satellite merging techniques applied in its predecessor Tropical Rainfall Measuring Mission (TRMM) Multisatellite Precipitation Analysis (TMPA) (Huffman et al. 2007). For this study, IMERG data are extracted from the reference period 2000–22, and half-hourly data are aggregated to 0800–0800 UTC daily accumulations, consistent with RG 24 accumulations. The extremeness of the 18–19 June 2018 event was evaluated in a percentile-based analysis by comparing its daily rainfall to all available June daily amounts from the reference period, considering only nonzero rainfall (≥1 mm).

d. Clouds and MCS tracked data

Convective cloud features were identified using the infrared (IR) brightness temperature dataset (channel 9 at approximately 10.8 μm) from the Spinning Enhanced Visible and IR Imager (SEVIRI) on the Meteosat Second Generation (MSG) satellite (Aminou 2002) operated by the European Organisation for the Exploitation of Meteorological Satellites (EUMETSAT). These datasets are available at 3-km spatial and 15-min temporal resolutions. Convective systems over West Africa have been detected employing a commonly used brightness temperature (T_b) threshold < 241 K (e.g., Arkin 1979; Feng et al. 2021). SEVIRI data from 17 to 20 June 2018 are used in the present work.

During the same time span, tracking data from a global MCS dataset created by Feng et al. (2021) are used. The database combines half-hourly 4-km global merged IR V1 T_b (Janowiak et al. 2001) from National Oceanic and Atmospheric Administration (NOAA) and National Centers for Environmental Prediction (NCEP) and hourly GPM IMERG V06B data at a spatial resolution of 0.1° × 0.1° (Tan et al. 2019; Huffman et al. 2020), allowing for an in-depth monitoring of the produced rainfall generated by each tracked MCS. For more details about the tracking algorithm, the reader is referred to the extensive descriptions given in Feng et al. (2021).

Microwave (MW) data at high-frequency bands, such as 89 or 157 GHz, provide more insight into the frozen and potentially precipitation-forming hydrometeor content of clouds since microwave signals at these frequencies are strongly attenuated by ice particles (e.g., Wilheit 1986; Muller et al. 1994). Thus, GPM MW Imager (GMI) and the MW Humidity Sounder (MHS) from the polar-orbiting satellites of the NOAA are utilized to investigate the characteristics of the relevant cloud systems before and during the extreme event. The channels ranging from 10 to 89 GHz have been used to indirectly infer rainfall in low T_b areas (Hou et al. 2014; Draper et al. 2015; Skofronick-Jackson et al. 2017). The 157-GHz channel of MHS and the 89-GHz channel of GMI are used for the analysis, the former of which is particularly used for its reduced noise levels (Redl et al. 2015).

e. Vorticity budget

Using ERA5 data, each term of the vorticity tendency equation (VTE) is analyzed to identify sources of relative vorticity during the passage of MCS over the study region. Since the focus is on investigating a potential vortex development in the lower troposphere, the layer between 1000 and 600 hPa is considered. The local temporal change in relative vorticity in the pressure (p) coordinate system at each grid point is formulated as

$$\frac{\partial \zeta}{\partial t} = -\mathbf{v}_h \cdot \nabla \eta - \omega \frac{\partial \zeta}{\partial p} - \eta \nabla \cdot \mathbf{v}_h + \mathbf{k} \cdot \left(\frac{\partial \mathbf{v}_h}{\partial p} \times \nabla \omega \right), \tag{1}$$

where ζ, f, and $\eta = \zeta + f$ are the relative, planetary, and absolute vorticity, respectively. The $\nabla = (\partial/\partial x)\mathbf{i} + (\partial/\partial y)\mathbf{j}$ ($\mathbf{i}$ and $\mathbf{j}$ are the unit vectors in the east and north directions, respectively) is the horizontal gradient operator. The $\mathbf{v}_h = u\mathbf{i} + v\mathbf{j}$ denotes the horizontal wind vector, ω is the vertical wind, and $\mathbf{k}$ represents the vertical unit vector. The first two terms on the right-hand side represent the horizontal advection (HADV) and vertical advection (VADV) of relative or absolute vorticity, respectively. The third term is the divergence (DIV) term and indicates changes in local relative vorticity by horizontal divergence in nonzero absolute vorticity field, characterizing the vortex stretching effect. Finally, the fourth term represents changes in relative vorticity resulting from a tilting (TILT) of a horizontal vorticity axis of preexisting vertical shear vorticity through nonuniform horizontal distribution of vertical motion. We refer to, e.g., Smith (1983), Holton and Hakim (2013), and Tory et al. (2012) for a detailed derivation of the VTE and its application as a diagnostic tool, respectively.

f. EFI and SOT

The EFI [see Eq. (S1)] measures the difference between ENS and the lead-time-dependent model climate (M-climate) and provides an indication of the likelihood of extreme

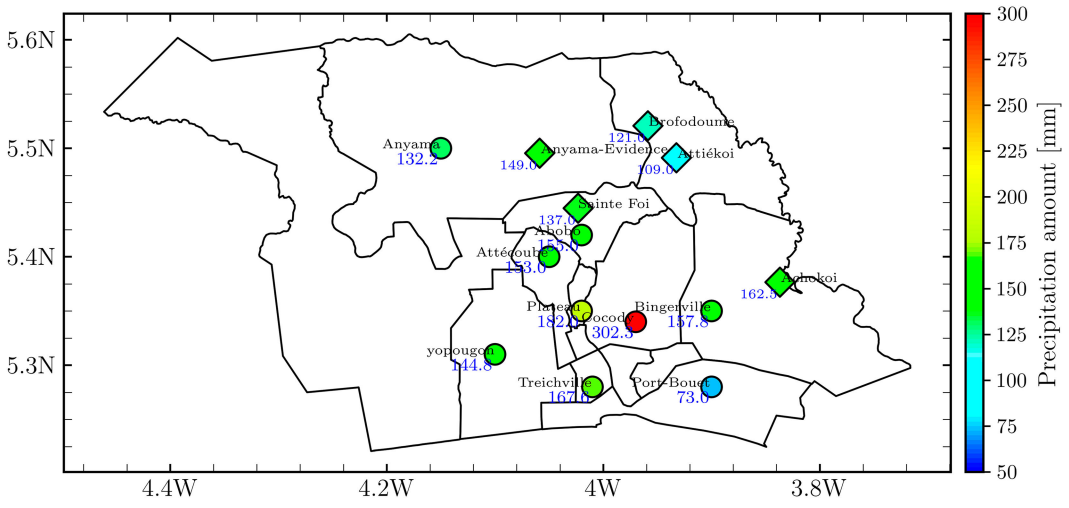

FIG. 2. The 24-h rainfall (mm) recorded by stations on 18–19 Jun 2018 from SODEXAM (circles) and EVIDENCE (diamond markers). These rainfall amounts were aggregated in the period 0800–0800 UTC.

weather conditions (Lalaurette 2003; Lavers et al. 2014; Tsonevsky et al. 2018). In the case of this paper, it refers to precipitation. The EFI values range from −1 to 1, which would indicate that all members are predicting a precipitation event unusually weaker (stronger) than the M-climate. An event is considered "unusual" or "very unusual" for EFI values between 0.5 and 0.8 or above 0.8, respectively. The SOT [see Eq. (S2)], introduced by Zsótér (2006), complements the EFI by providing additional insight into the magnitude of the extremity of an extreme precipitation event. It shows how extreme the tail of a given ensemble is compared to the tail of the M-climate distribution (Boisserie et al. 2016; Raynaud et al. 2018). Positive values of the SOT signify that at least 10% of the ensemble members are beyond the M-climate extreme (Tsonevsky et al. 2018).

3. Results and discussion

a. Spatiotemporal evolution of the extreme rainfall event

On 18–19 June 2018, the District of Abidjan experienced one of the highest registered daily precipitation events which was notable for its widespread impact such as extensive urban flooding (Amouin et al. 2021; Attoumane et al. 2022). The recorded precipitation from SODEXAM and EVIDENCE stations revealed varying amounts across different areas of the District of Abidjan (Fig. 2). The highest rainfall amount was reported at the Cocody station with 302 mm (Amouin et al. 2021). The closest stations from Cocody (approximately 13 km) reached 157 mm (Bingerville) and 182 mm (Plateau), highlighting considerable rainfall variability at small spatial scales. This suggests very localized precipitation features and developments that are challenging to resolve for spaceborne observations and numerical weather prediction (NWP) alike.

To put the 302 mm at Cocody into a regional perspective, Fig. 3 shows a combined scatter–violin–boxplot of historical daily rainfall amounts at selected Ivorian synoptic stations and stations at coastal cities across West Africa, for which multidecade long time series are available (Fig. S1). Regarding the Ivorian stations (Fig. 3a), a comparison is made between coastal (blue colors) and inland stations (red colors) with a distance of at least 100 km from coastline. Evidently, the distribution at the extreme end is considerably different between the two regions. More than 300 mm of rainfall are exclusively found at the coast, whereas 150 mm, rarely exceeded in historical records, can be considered as extreme for the inland stations. Up until the present extreme event, more than 302 mm in the District of Abidjan has been registered only once on 21 June 1983 (311 mm) within the available rainfall records dating back to 1936 (see Fig. S1). When compared to other coastal stations across West Africa (Fig. 3b), where 200 mm is already exceptional, rainfall amounts higher than 300 mm are virtually unique to Côte d'Ivoire. Thus, the extremity of the present precipitation event cannot be overstated.

Between 0000 UTC 18 June and 0000 UTC 20 June 2018, Fig. 4 illustrates the evolution of hourly rainfall and its cumulation at the five Abidjan EVIDENCE stations as well as at the closest IMERG and ERA5 pixels. Here, the rainfall accumulation curves start at 2200 UTC 18 June (i.e., representing the approximate onset of rainfall). On average, IMERG and ERA5 underestimate the daily rainfall by nearly half of that seen by the stations. This is unsurprising given the known challenges to capture both local enhancements of rainfall due to the point-to-pixel limitation (Ageet et al. 2022) and warm rain events (Maranan et al. 2020). The highest recorded precipitation amounts by any of the EVIDENCE stations are observed at Achokoi with nearly 163 mm (Fig. 4a), while approximately 70 mm is estimated at the corresponding IMERG and ERA5 grid points. However, the 99th percentile of 12-h accumulated rainfall, roughly the duration of the precipitation event, is exceeded in both IMERG and ERA5 during this event (red and green dashed horizontal lines, respectively), which also applies to all the other locations. Thus, despite the general underestimation, the 12-h intensities during this

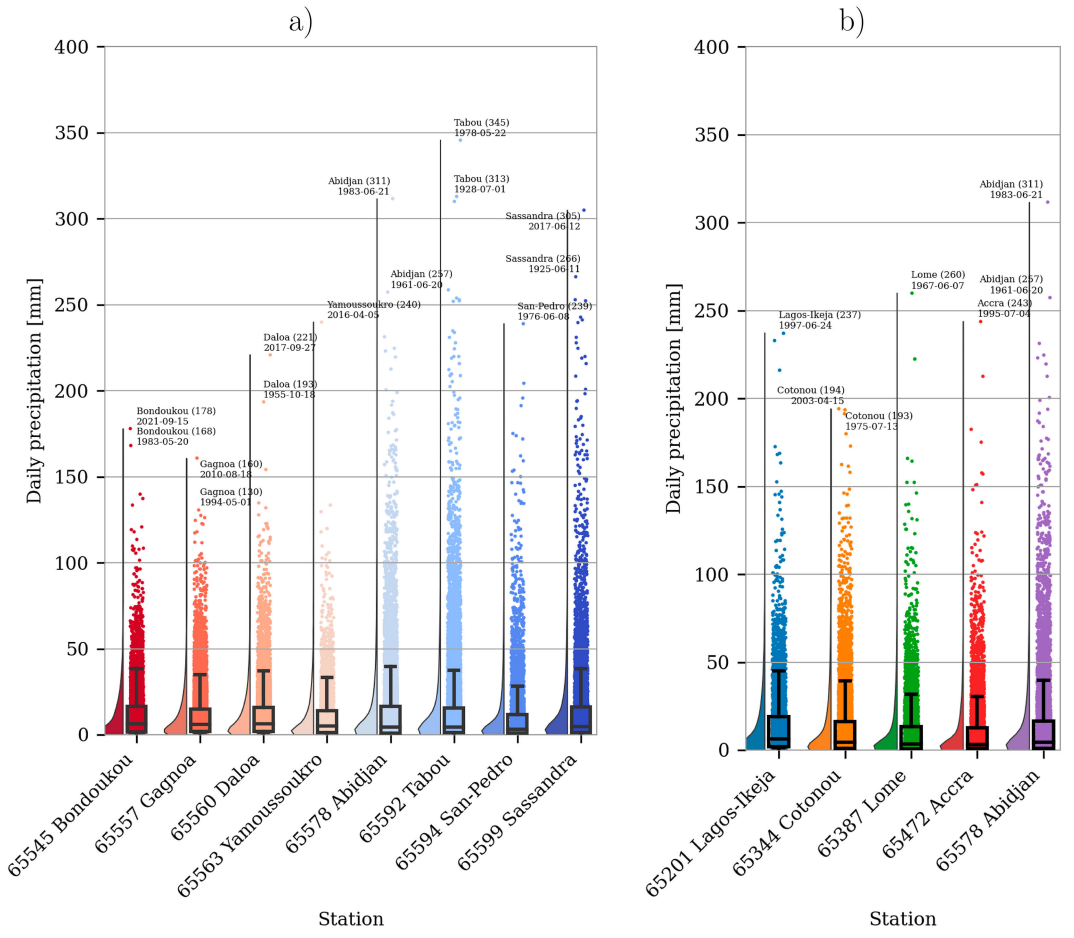

FIG. 3. Combined scatter–violin–boxplots of historical daily precipitation amounts (mm) for selected synoptic stations (WMO station IDs indicated in the labels) (a) in Côte d'Ivoire and (b) at large coastal cities across WA. In (a), red shading refers to inland cities and blue refers to coastal. Note that zero values were not included. For each station, the highest recorded daily rainfall values are annotated together with the dates. The station locations are indicated in Fig. 1a. Furthermore, the data availability is provided in Fig. S1.

extreme event belong to the highest in the entire IMERG and ERA5 samples at the respective grid points (99.5th and 99.9th percentiles, respectively).

Furthermore, comparing the temporal evolutions of hourly rainfall, the first 2 h are considerably more intense in the station data (blue bars in Figs. 4a–e) than in IMERG, the latter of which "agrees" on a maximum between 0300 and 0400 UTC (red bars). Intermittent peaks of intense rainfall are notable only in the stations as well, generally occurring between 0000 and 0600 UTC 19 June. In contrast, the rainfall event in IMERG persisted until past noon and, thus, was around 5 h longer than measured by the stations. Note that ERA5 lacks intensity and timing of the rainfall (i.e., lag of 5–6 h) compared to the stations which, to first order, is likely attributable to the coarse horizontal resolution, as elucidated in, e.g., Magnusson et al. (2019). This reflects the ongoing challenges of representing the spatiotemporal characteristics of local convection. Furthermore, we already note here that the most extreme rainfall in ERA5 associated with the present case did not exactly occur over the District of Abidjan but slightly to the southwest (see Fig. S2). While being a demanding task for the parameterization-based ERA5 short-term rainfall forecast to capture this event satisfactorily in space, time, and intensity, the fact that IMERG struggles as well is again indicative for the exceptional local-scale variability of extreme rainfall. This spatiotemporal mismatch will be accounted for and further discussed in the anticipation of the analysis of (thermo)dynamical fields performed in later sections. Nonetheless, as the most intense period of rainfall occurred before 0600 UTC in both RG and IMERG datasets, the focus of the analysis in the following is put between 1800 UTC 18 June and 0600 UTC 19 June.

To obtain an overview of the regional context of the extreme rainfall event across West Africa, Fig. 5 shows daily IMERG fields on 18 June and 19 June, as well as the 48-h accumulated rainfall for 18–19 June (left column). Furthermore, the percentile values at each pixel based on the period of June 2001–22 are shown (right column). Based on the spatial rainfall pattern, it is discernible that the extreme event is a consequence of a westward-moving precipitation signal that approaches the District of Abidjan (star marker) on 18 June

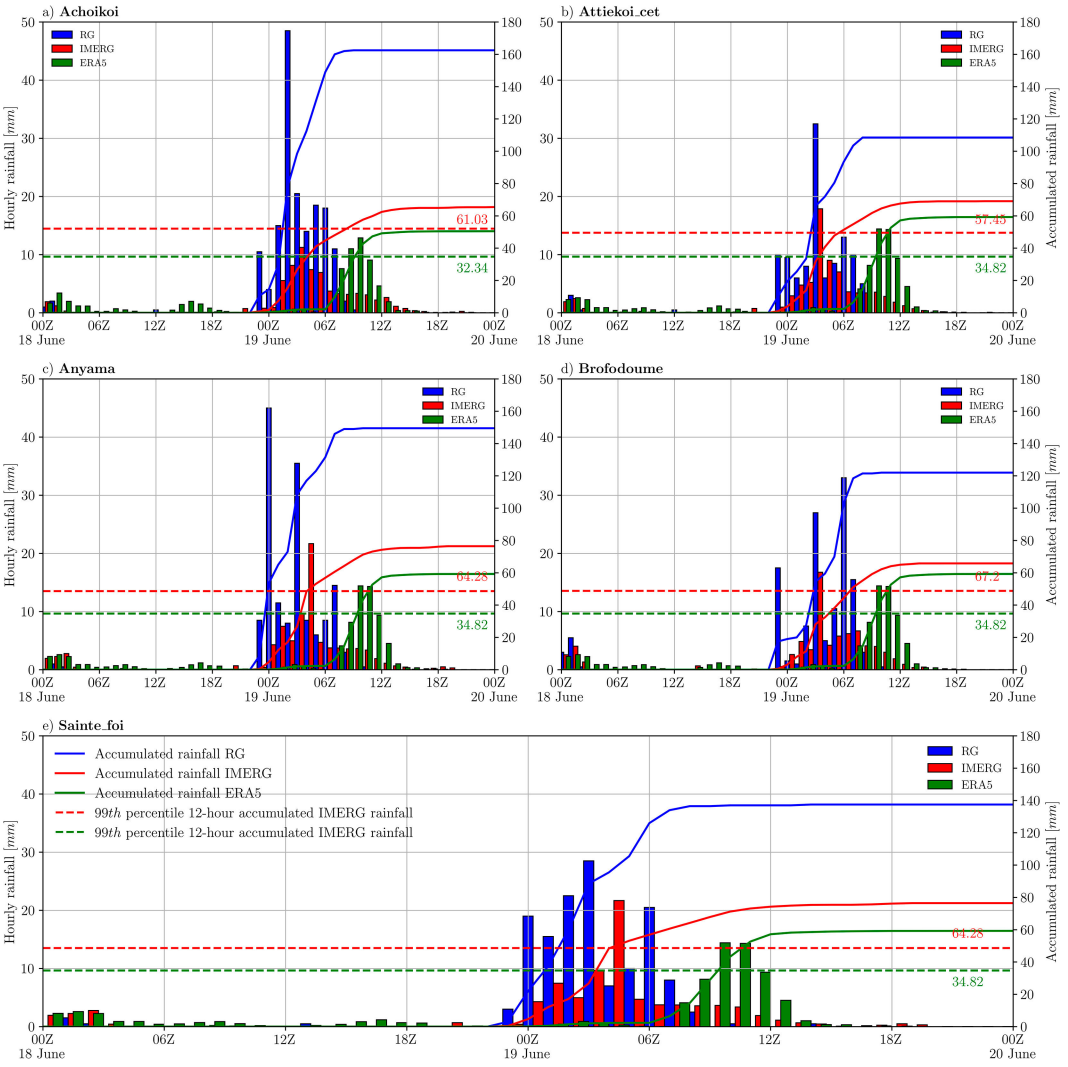

FIG. 4. Hourly rainfall distribution in RG observations (blue bars), IMERG (red), and ERA5 (green) from five Abidjan EVIDENCE stations (Zahiri et al. 2023) and the closest IMERG/ERA5 grid points, respectively: (a) Achokoi, (b) Attiekoi_cet, (c) Anyama, (d) Brofodoume and (e) Sainte_foi. The respective solid curves correspond to the hourly evolution of the cumulative precipitation from 2200 UTC 18 Jun to 0000 UTC 20 Jun 2018. The curves represent the event accumulations only. Red and green dashed lines represent the 99th percentile of the 12-h accumulated rainfall amount in IMERG and ERA5, respectively. The percentile is computed from nonzero rainfall using the long-term period June 2001–22 for IMERG and June 1991–2020 for ERA5 rainfall.

(Fig. 5a). On 19 June, this system continued its westward propagation further toward the eastern Atlantic (Figs. 5c,e). Overall, the highest rainfall amounts over the course of both days are found over the offshore region of the Guinea Coast (Fig. 5e). Enhanced onshore rainfall in the District of Abidjan up to 100 mm is evident but does not necessarily surmise conditions for an extreme event (in terms of absolute values) in the same fashion as the station data. However, considering the percentile values (Figs. 5b,d,f), most IMERG grid points in the District of Abidjan exhibit maximum percentile values and underline extreme amounts within the sample of the 2001–22 IMERG reference period.

b. Cloud characteristics of the rainfall systems

Figure 6 shows IR-based snapshots from SEVIRI at key stages of the development of the rainfall system (red boxes) responsible for the extreme rainfall over the District of Abidjan, with $T_b < 241$ K, i.e., a proxy for tropical deep convection, shown in rainbow colors. This intense rainfall event was caused by a long-lasting MCS which formed over the Cameroon Highlands at around noon on 17 June (Fig. 6a), rapidly propagated southwestwards and crossed the Nigerian shoreline past midnight on 18 June (Fig. 6b). During this stage and the propagation over the ocean along the Guinea Coast over the course of 18 June (termed "oceanic phase"), the MCS grew in size and

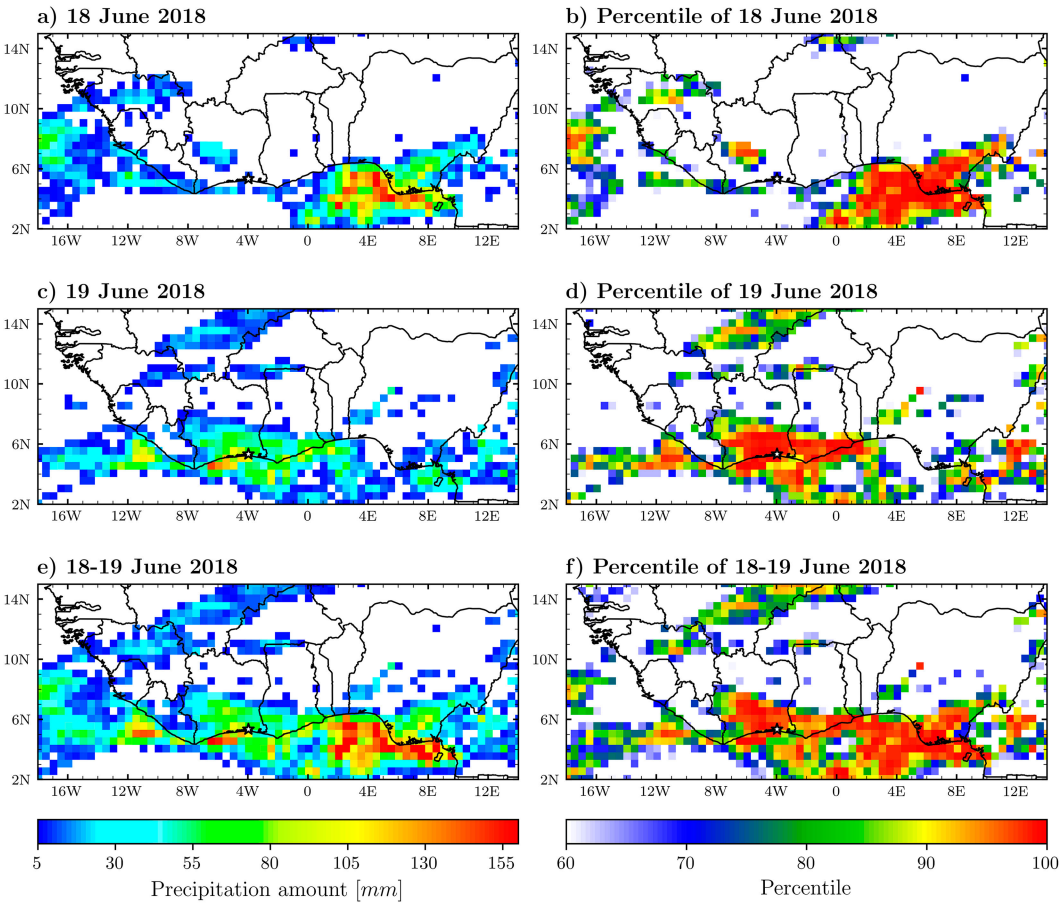

FIG. 5. Spatial distribution of (left) IMERG precipitation (mm) and (right) the corresponding percentiles with respect to 24-h accumulations on (a),(b) 18 Jun 2018 and (c),(d) 19 Jun 2018 and 48-h accumulation on (e),(f) 18–19 Jun 2018. The black star marker shows the location of the District of Abidjan (e.g., 5.34°N, 3.97°W). The percentiles are computed using only rainy days (daily amounts ≥ 1 mm) over the long-term period June 2001–22.

intensified, forming a broad and a deep cell with a core T_b at around 190 K (Figs. 6c,d). This is in accordance with intense oceanic rainfall at 3°E seen by IMERG in Figs. 5a and 5e. As the MCS crossed the zero meridian and made "landfall" at the Ghanaian coast during the evening of 18 June, causing damages in Accra (Osei et al. 2023), it began to weaken, indicated by decreasing size and increasing core T_b (Fig. 6e). Before the MCS reached the District of Abidjan region at around 0100 UTC 19 June (Fig. 6f), small convective cells were already present there which formed in the late evening of the previous day (not shown). These relatively shallow cells likely caused the early spikes in the records of the EVIDENCE stations (e.g., at Anyama and Brofodoume, Figs. 4c,d), while largely not being detected by IMERG (Fig. 5), and eventually merged with the approaching MCS from the east at around 0300 UTC (Fig. 6g), coinciding with the hourly rainfall maximum in IMERG (Fig. 4). This convective cluster eventually featured an extensive residence time over the coast of Côte d'Ivoire (Figs. 6f–i; see also Fig. S3), up to 10 h according to the station rainfall records (Fig. 4) before it moved further west toward the late morning of 19 June (Fig. 6j). Overall, despite an apparent weakening of the MCS, according to the increased T_b as it approached the District of Abidjan region, it remarkably caused one of the most intense daily rainfall amounts in Abidjan on record with considerable contrasts in cloud features compared to the convective systems in Engel et al. (2017) and Maranan et al. (2019).

Figure 7 summarizes cloud and precipitation features of the MCS over the course of its lifetime. The cloud extent, defined by the 241-K envelope, as well as the minimum T_b at every time step during its lifetime, is illustrated in Fig. 7a. As indicated before, the MCS is largest and deepest during its oceanic phase after a rapid spatial expansion upon initiation over the Cameroon Highlands. Likewise, the first two snapshots from MW imagery by GMI and MHS on 17 and 18 June, respectively, along the MCS track reveal cold T_b as low as 120 K (Fig. 7b), suggesting the presence of abundant ice particles within the convective cloud. The radiometrically warmest and, thus, shallowest phase during the existence of the MCS indeed occurs during the passage over the District of Abidjan (Figs. 7a,b), which likely explains the lower accumulated

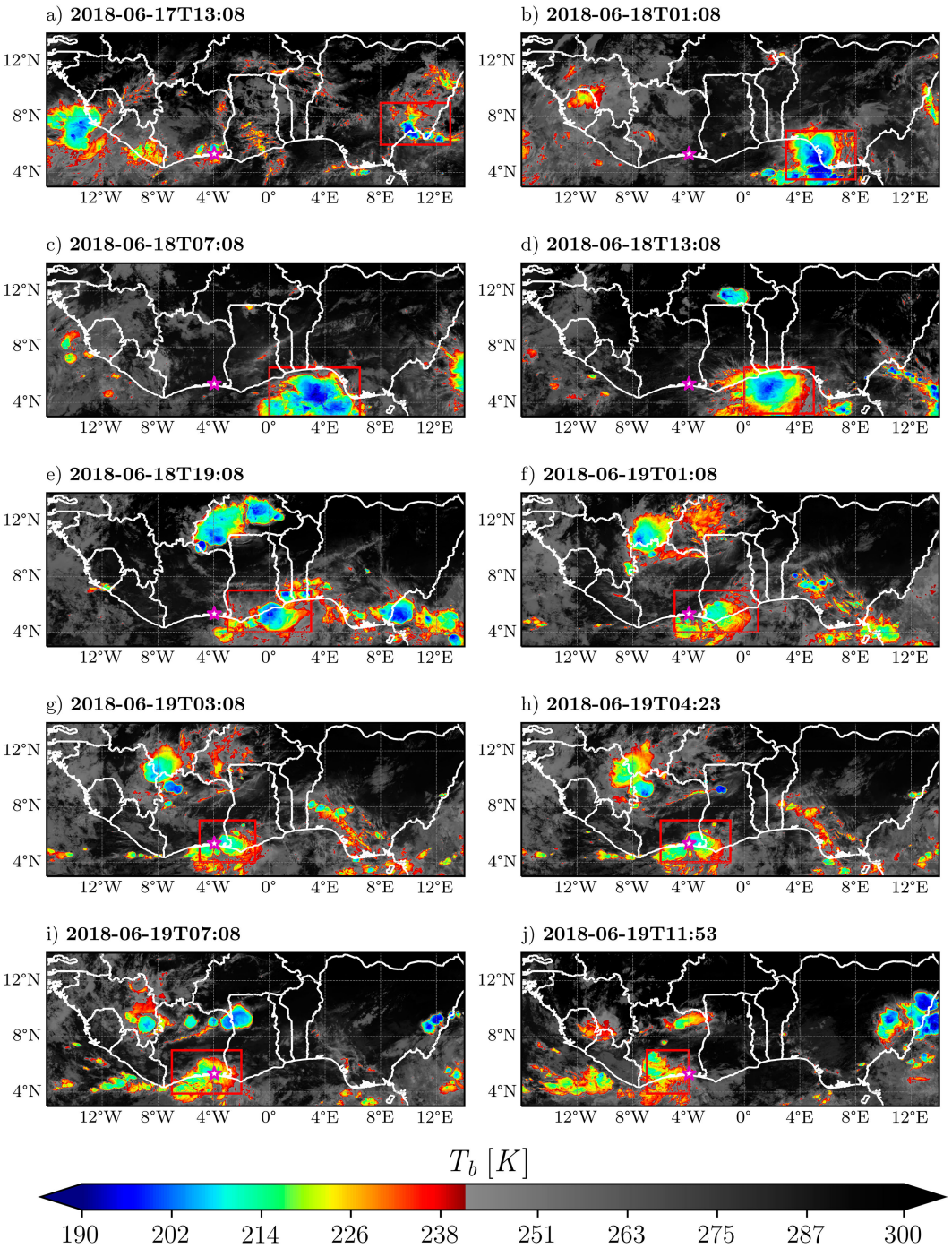

FIG. 6. SEVIRI IR brightness temperature (T_b) fields (channel 9 at approximately 10.8 μm) over WA at key time steps of the life cycle of the MCS (red box for spatial reference) that caused the extreme event. This red box was manually drawn to highlight the location as well as the extent of the MCS. Here, the rainbow color scale denotes T_b below 241 K. The purple star represents the District of Abidjan (i.e., 5.34°N, 3.97°W).

IMERG rainfall amounts in this area compared to the oceanic phase (Fig. 7c). More insight into the hourly evolution of properties of the MCS during its life cycle regarding size (black curve), the minimum T_b (blue), and average IMERG precipitation rate of nondry pixels within the MCS envelope (red) is presented in Fig. 7d. The red, dashed vertical lines denote the period where, according to the IMERG rainfall signals, the MCS was active over the District of Abidjan from

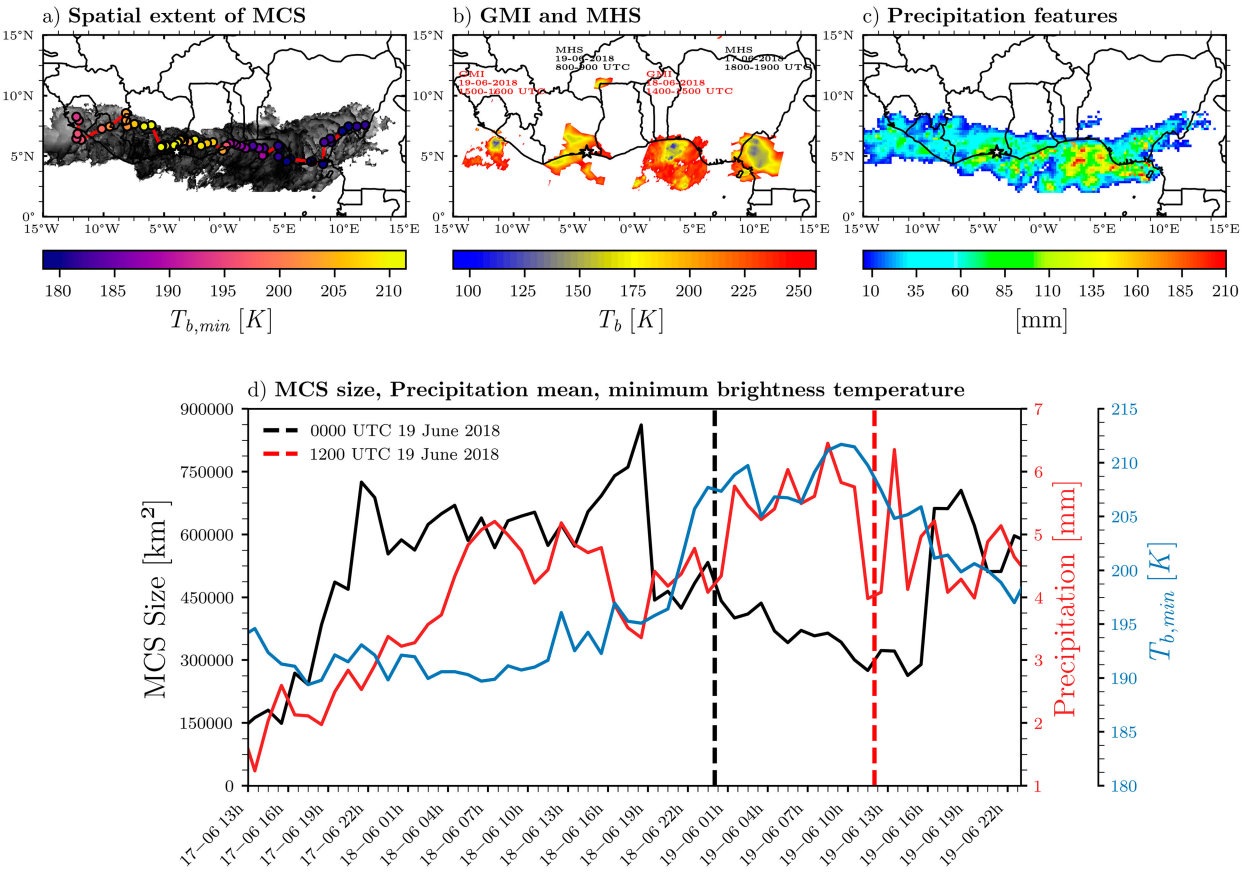

FIG. 7. (a) Cloud characteristics showing the spatial extent of the MCS as well as the minimum brightness temperature across the entire cloud-top area at all available time steps ($T_{b,\min}$). (b) GMI (157 GHz) and MHS (89 GHz) brightness temperature (K) over WA at different dates. (c) Estimated accumulated IMERG precipitation within the 241-K envelope of the MCS during the time of the overpass, see (a). (d) Temporal evolution of MCS size (black), mean precipitation of nondry IMERG pixels within the MCS envelope (red), and minimum brightness temperature.

0000 to 1200 UTC 19 June (cf. Fig. 4). The growth of the MCS in size over time ended with a sudden shrinking at 1800 UTC 18 June, mainly due to a splitting of the convective cloud cluster. Toward and during the overpass over the District of Abidjan, the structural weakening of the MCS is visible through the decrease and increase in size and minimum T_b, respectively. Again, the latter indicates that the MCS becomes gradually shallower over time. Despite that, the average hourly precipitation rate of rainy IMERG pixels is highest during the passage over the District of Abidjan, suggesting an ongoing production of enhanced rainfall. Potential reasons for this are evaluated with ERA5 in the upcoming sections.

In this regard, the question whether ERA5 actually captures the existence of the MCS is briefly addressed in Fig. S4, which shows the presence of extensive MCS-related cold cloud feature as well as its weakening in both IFS forecast and reanalysis during the oceanic phase and over the coastal region of Côte d'Ivoire, respectively. As this resembles the observed evolution of the MCS, it provides confidence that reasonable insights on the atmospheric setting around the extreme event can be drawn from ERA5.

c. *Local- to regional-scale evolution of the extreme event*

1) DEVELOPMENT OF MOISTURE AND RAINFALL ON THE LOCAL SCALE

Figure 8 presents the time series of MFC and hourly RG and IMERG rainfall (left column) and PW and ERA5 rainfall (right column) for the period 18–20 June 2018. Figures 8a and 8b, the variables are averaged within a 1° × 1° box around the District of Abidjan (see purple box in Fig. 1a). Considering the occurrence of rainfall seen by the stations and IMERG, the MCS impacted the District of Abidjan roughly within a 12-h period between 0000 and 1200 UTC 19 June 2018 (Fig. 8a). In this time span, MFC (solid red curve) features a pronounced intensification and peaks at 0700 UTC at around 300 mm day^{-1}. This by far exceeds the 30-yr-based (1991–2020) 99th percentile (dashed red curve) at that particular hour and cannot be explained by regular processes of the diurnal cycle, the latter of which usually peaks in the afternoon at 1500 UTC. The increase in ERA5 rainfall from 0600 UTC onward, shown in Fig. 8b and at its peak beyond the 99th percentile (black dashed curve) as well, is evidently linked to the intense spike in MFC. However,

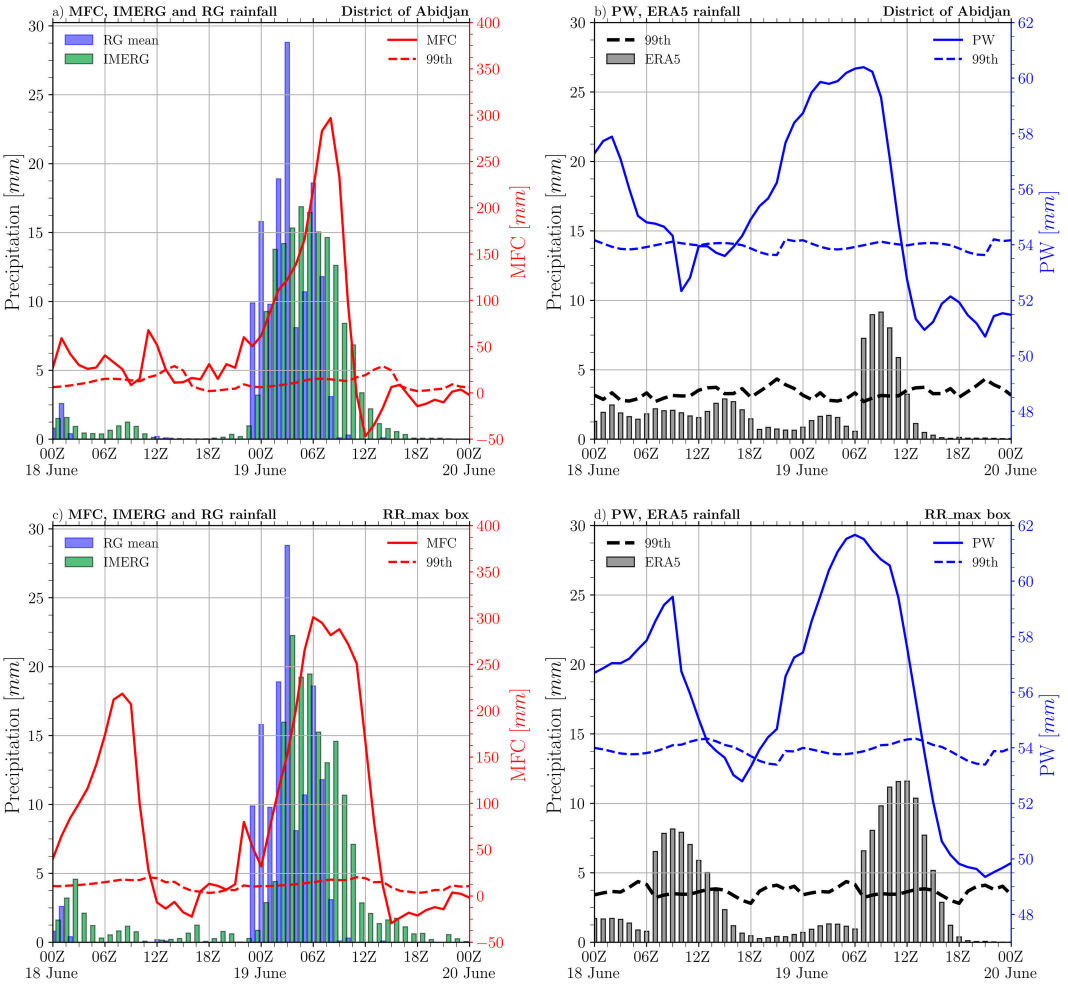

FIG. 8. Time series between 0000 UTC 18 Jun and 0000 UTC 20 Jun of (a),(c) hourly RG and IMERG rainfall (blue and green bars) and hourly column-integrated MFC (solid red line) and its long-term (i.e., June 1991–2020) 99th percentile at each hour of the day (dashed red line) and (b),(d) hourly ERA5 rainfall (gray bars) and hourly PW (solid blue line) and its long-term (i.e., June 1991–2020) 99th percentile at each hour of the day (dashed blue line). The quantities in (a) and (b) are averaged within a 1° × 1° box around the District of Abidjan (see purple box in Fig. 1) and in (c) and (d) are averaged within a 1° × 1° box around the location of RR_max (see orange box in Fig. 1).

the foundation for an extreme event was laid hours before the MFC and ERA5 rainfall peaks, with PW exhibiting a distinct increase well beyond the hour-based 99th percentile (dashed blue curve) during the evening on 18 June (Fig. 8b).

While ERA5 generally shows the indications of conducive environmental controls for enhanced precipitation over the District of Abidjan, the mismatch with respect to timing and rainfall intensity and duration compared to the observations again highlight the challenges in capturing the extreme nature of the event, owing to its small-scale spatial variability and the inherent limitations of the convection parameterization within IFS in resolving it. In fact, the most intense rainfall in ERA5 did not occur over the District of Abidjan but slightly to the southwest of it (see Fig. S2). Here, Figs. 8c and 8d show the conditions within the 1° × 1° domain around the location of the maximum ERA5 rainfall (termed RR_max; for spatial reference, see orange box in Fig. 1a). Owing to the westward displacement of the analysis domain in relation to the District of Abidjan, the peaks of MFC (Fig. 8c) and PW (Fig. 8d) occur 1–2 h later but are of comparable magnitude. However, ERA5 rainfall peaks at higher values (Fig. 8d) and exhibits an event duration of around 12 h that is closer to that of IMERG (see Fig. 8a).

Overall, the initial choice of the analysis domain over the District of Abidjan was impact driven based on the extreme rainfall values in the rain gauge data, but it is not entirely known whether the maximum rainfall associated with the MCS actually occurred there due to the lack of further ground-based observations. Both IMERG (see Fig. 5c) and ERA5 (Fig. S2) suggest a slight displacement of the rainfall maximum to the southwest which, however, must be considered with obvious uncertainties in remotely sensed precipitation estimation and model-driven and parameterized convective rainfall, respectively. Thus, while acknowledging a potential spatiotemporal

mismatch of the extreme event in ERA5 compared to the rain gauge observations, the considerable excess of rainfall beyond the 99th percentile supports the presumption that ERA5 reasonably depicts the extreme event in general. To facilitate a process-oriented analysis of how the most extreme rainfall might have been generated, the study of the environmental settings will now focus—unless noted otherwise—on the domain of the maximum ERA5 precipitation in the following sections.

2) Synoptic-scale analysis of the environmental setting around the extreme event

Expanding on the previous section, moisture-related and dynamical fields around the extreme event are evaluated via Hovmöller diagrams ranging across the Guinea Coast region (Fig. 9). Here, the fields are averaged within the 4.25°–5.75°N latitudinal band, i.e., roughly centered along the zonally oriented coastline of Côte d'Ivoire. The longitudinal extent of both the District of Abidjan and the domain of maximum ERA5 rainfall, as well as the period of the extreme event, are framed by the dashed black vertical and horizontal lines, respectively. Linked with the westward propagation of the MCS (see Fig. 6), a clear westward-moving signal of MFC, PW, and IMERG precipitation, originating as far east as 10°E in the late evening of 17 June, is visible (Figs. 9a–c), indicating that the existence of moist conditions and a long-lived MCS are highly intertwined in this case study. During the oceanic phase of the MCS east of the zero meridian, all three parameters were extreme, shown by extensive high percentile values in Figs. 9d–f and which is in line with intense offshore precipitation amounts (see Fig. 5a). However, while the westward-moving MFC and PW signatures slightly weaken before the arrival in the study region, both experience an enhancement in magnitude over the study area (Figs. 9a,b). Furthermore, dynamical fields, represented by the 700-hPa relative vorticity, divergence, and vertical velocity, respectively, indicate pronounced cyclonic and convergent motions, i.e., a low-tropospheric moist vortex, potentially related to strong updrafts in the District of Abidjan region (Figs. 9g–i). This intensification of the dynamical parameters does not necessarily align with the structural weakening of MCS (cf. Figs. 6 and 7), suggesting that the strengthening of the moist vortex played a critical role in triggering the extreme rainfalls. Further hints of the existence of a vortex are seen in the 950–600-hPa-based LLWS Hovmöller field (Fig. S5). Flanked by preceding enhanced LLWS in time, it features a "swath" of a weak LLWS signature propagating in accordance to the MFC and PW patterns. This is presumably indicative of the eastern flank of the vortex center.

Finally, it remains to be noted that the vortex is likely not part of an AEW. Having applied the AEW tracking tool of Fischer et al. (2024) on the present case, no definite AEW pattern along the Guinea Coast before and during the extreme event was identified by the algorithm which is most likely due to the lack of a clear wave trough structure in the 700-hPa wind field (see Figs. S6a–d). Instead, it can be argued that the vortex is a disturbance that is primarily tied with the existence of the MCS.

Regional-scale snapshots of MFC, VIMF, PW, the mass-weighted low-level flow (see section 2b), and the LLWS field at 6-hourly time steps prior to the extreme event are shown in Fig. 10. Note that the last time step, i.e., 0600 UTC 19 June, coincides with the onset of intense rainfall in ERA5 (cf. Figs. 8b,d) and is, therefore, still representing "preevent" conditions. For the spatial reference of the observed MCS and the study area, their position and extent at the respective time steps are indicated with the 241-K-based blue contour and orange box, respectively. Here, the potential interaction between MCS and the moisture field becomes evident through enhanced MFC and PW signals close to the location of the MCS. On the eve of the extreme event over the District of Abidjan on 1800 UTC 18 June 2018, the entire Guinea Coast is influenced by pronounced southwesterly moisture flux and that is concentrated offshore of Benin and Nigeria (Figs. 10a,b) with collocated PW values beyond 60 mm. Signatures of a cyclonic circulation trapping high loads of moisture, i.e., a moist vortex, is already apparent in the low-level flow and can be associated with the intense oceanic rainfall (see Fig. 5a). While it is not entirely clear where exactly the influence of the MCS (i.e., in the form of MCS-related upper-level divergence in the assimilated atmospheric motion vector field) is assimilated within ERA5 in terms of location, high MFC and PW values continue to appear alongside the cyclonic flow in the subsequent time step at midnight on 19 June (Figs. 10d,e), before intensifying over the District of Abidjan region at 0600 UTC (Figs. 10g,h). This time step highlights a well-developed vortex with its center over the study region and is directly linked to the extreme local peaks in MFC and PW seen in Fig. 8. As mentioned above, the fact that over 300 mm within only several hours was produced with a relatively warm, i.e., shallow, MCS (see Fig. 7a) is indicative of the importance of moisture refueling capabilities of such moist vortices.

With respect to the LLWS fields, areas of enhanced wind shear (red shaded areas) and, thus, generally conducive conditions for convective intensification are visible along the Guinea Coast ahead of the westward-moving MCS prior to the extreme event (Figs. 10c,f). By the time the MCS reaches the study region, an extensive area of weak LLWS along the coast of Côte d'Ivoire is established (Fig. 10i). It can be speculated whether this indicates a modification of the wind field related to the intensified vortex. Overall, while enhanced LLWS has an undeniable positive impact on convective organization in West Africa in general (e.g., Taylor et al. 2017; Klein et al. 2021), its role on the MCS in the present case remains difficult to diagnose in detail, especially considering potential limitations of ERA5 in representing the mesoscale dynamics of convective systems. Nonetheless, since LLWS can be a source of vorticity generation, an attempt is made to quantify the contribution of LLWS to the budget of relative vorticity through the tilting term in the VTE, and thus the intensification of the vortex, in section 3c(3).

For the same time steps as in Fig. 10, zonal vertical cross sections of relative vorticity (left column) and vertical velocity (right column) averaged over 4.25°–5.75°N (i.e., latitudinal range of both boxes District of Abidjan and RR_max) provide

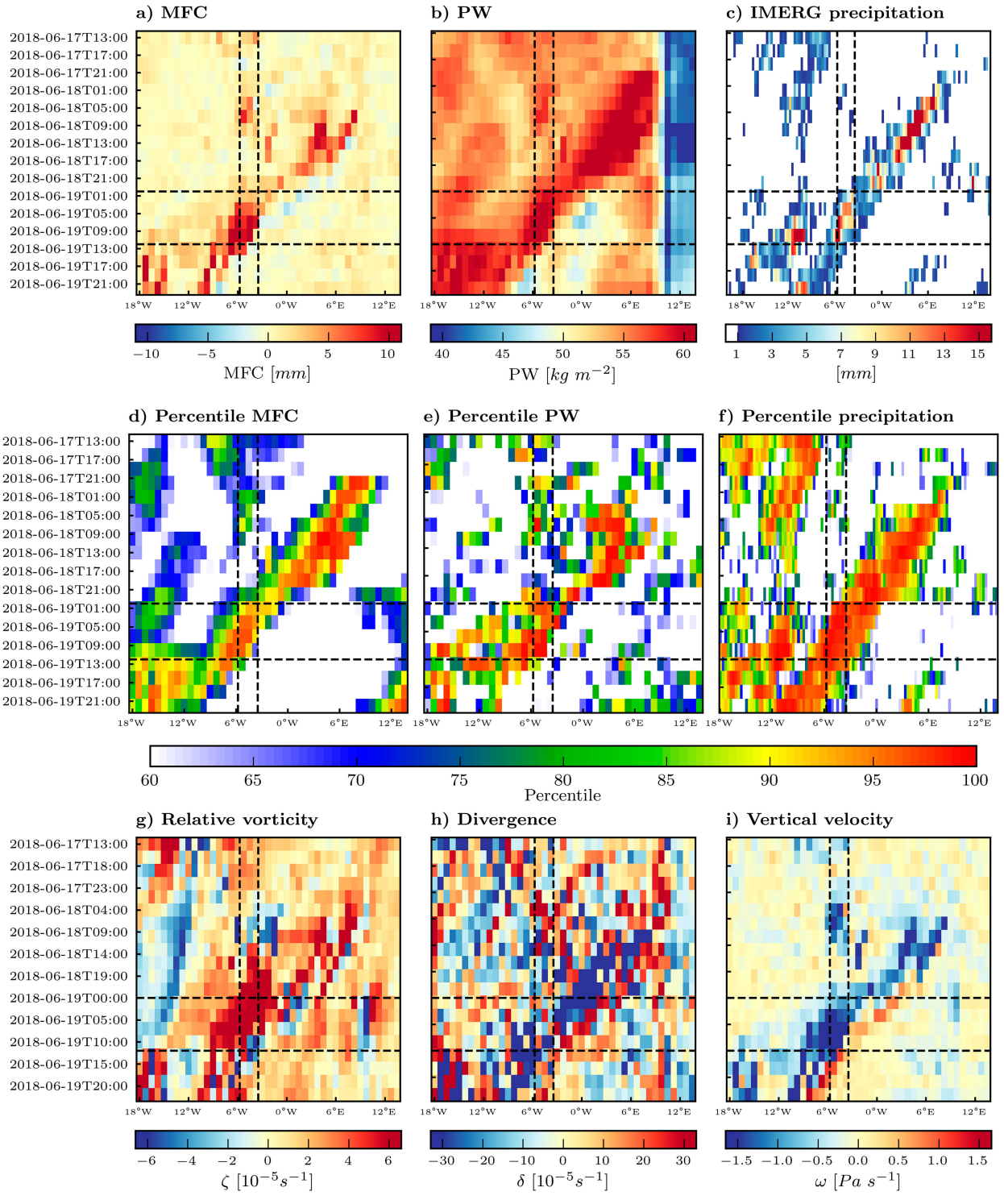

FIG. 9. Hovmöller diagrams of (a) MFC, (b) PW, and (c) IMERG precipitation. (d)–(f) The respective percentile values based on the June 1991–2020 climatology for MFC and PW and June 2001–22 for IMERG precipitation, respectively. (g) Relative vorticity, (h) DIV, and (i) vertical velocity (ω) at 700 hPa at hourly time steps from 1200 UTC 17 Jun 2018 to 0000 UTC 20 Jun 2018. All variables are averaged over the 4.25°–5.75°N latitude band. Vertical dashed lines indicate longitudinal extent of both the District of Abidjan and the domain of RR_max, while horizontal dashed lines denote the extended period of the extreme event (0000–1200 UTC 19 Jun 2018).

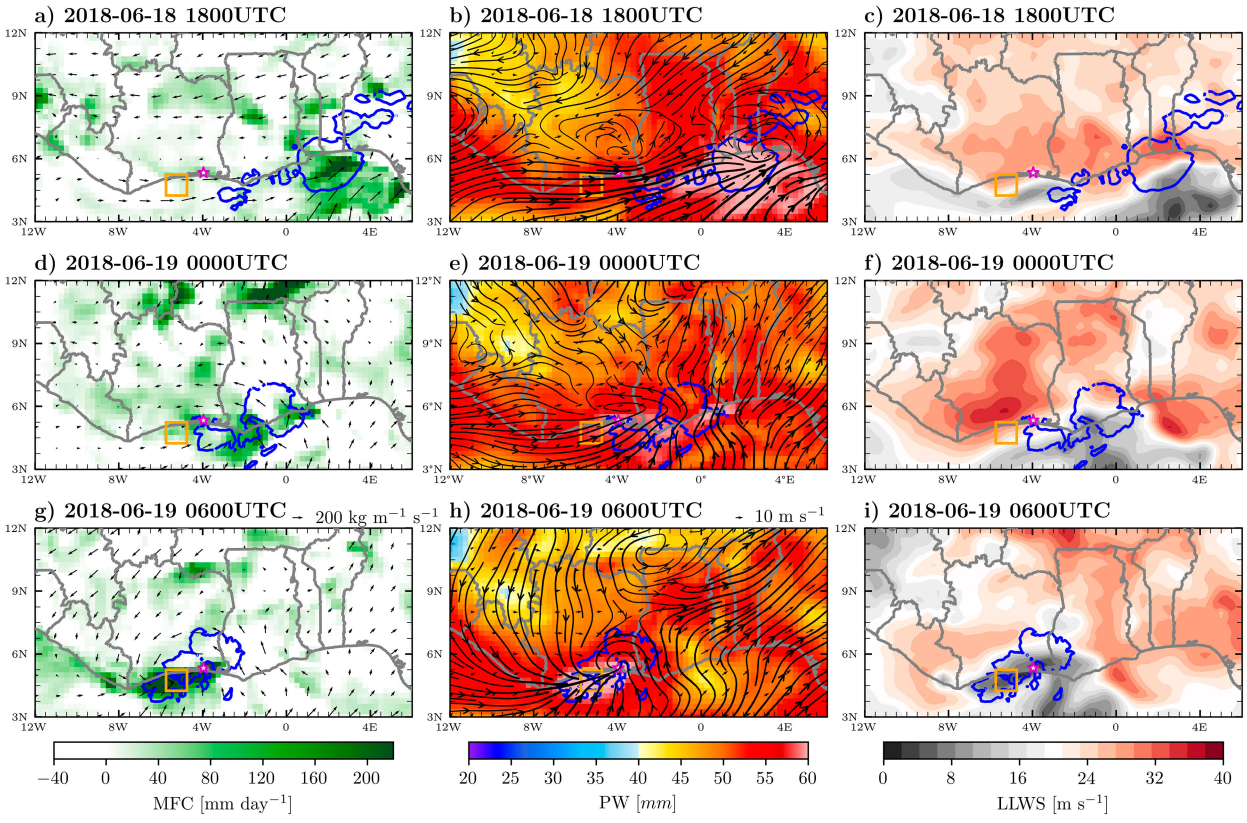

FIG. 10. Fields of (left) MFC (shaded; mm day^{-1}) and VIMF (vectors; kg m^{-1}s^{-1}); (middle) PW (shaded; mm), 600–950-hPa mass-weighted flow (streamlines), and low-level horizontal winds at 925 hPa (V_{925}, vectors; m s^{-1}); and (right) LLWS (shaded; in m s^{-1}) at the following time steps: (top) 1800 UTC 18 Jun 2018, (center) 0000 UTC 19 Jun 2018, and (bottom) 0600 UTC 19 Jun 2018. The blue contours show spatial extent of the MCS below 241-K threshold (see Fig. 7a); and the purple star indicates the District of Abidjan.

an impression of both the depth of the moist vortex and the associated vertical motions (Fig. 11). The x markers at the bottom of each of the subfigures show the zonal position of the MCS centroid in the observation. Here, the zones of strongest ascending motions appear to be linked to the MCS, an indication that the MCS-related dynamics are captured by the reanalysis. Furthermore, the appearance of the MCS is further supported by enhanced values of upper-level ice water contents (blue contours) as well as clear signatures of enhanced rainwater content in the lower troposphere (red contours). Overall, the pronounced westward-moving vertical motion signatures are strongly related to cyclonic structures, the depth of which considerably varies from one time step to the other. The oceanic phase at 1800 UTC 18 June (Fig. 11a) and the onset of the extreme event (Fig. 11e) prominently feature deep cyclonic "towers." As seen before, these time steps are in line with well-developed vortex structures in the low-tropospheric flow. One remarkable aspect of the vortex structure before the extreme event is its expansion down to levels at around 850 hPa (Fig. 11e) which coincides with distinct ascending motions that reach near-surface levels (Fig. 11f) and increased moisture convergence as shown in Fig. 10f. It is speculated that this downward development enhanced the uptake of abundant moisture in the low levels and, thus, increased the production of rainfall even with a weakening MCS.

3) ON THE EVOLUTION OF THE MOIST VORTEX OVER THE DISTRICT OF ABIDJAN REGION

The previous sections corroborated a correlation between an intensifying cyclonic low-tropospheric vortex and the formation of extreme rainfall along the coast of Côte d'Ivoire on 19 June 2018 despite the weakening of the approaching MCS it interacted with. Here, Fig. 12 delves deeper into potential processes that might have led to the pronounced manifestation of the moist vortex. It shows the hourly evolution of the vertically integrated VTE components [see Eq. (1)] from 1800 UTC 18 June to 1800 UTC 19 June. To evaluate potential processes behind the manifestation of the moist vortex, the VTE was applied on a 1° × 1° box centered around the area of maximum precipitation in ERA5 (i.e., 4.75°N, 5.25°W) before and during the onset of strongest rainfall. As mentioned before, the shift away from the District of Abidjan as the analysis domain accounts for the spatiotemporal mismatch of maximum ERA5 rainfall related to the event compared to observation. This way, more focused insight can be gained on processes that have likely facilitated the production of the most extreme rainfall, and here specifically in relation to the

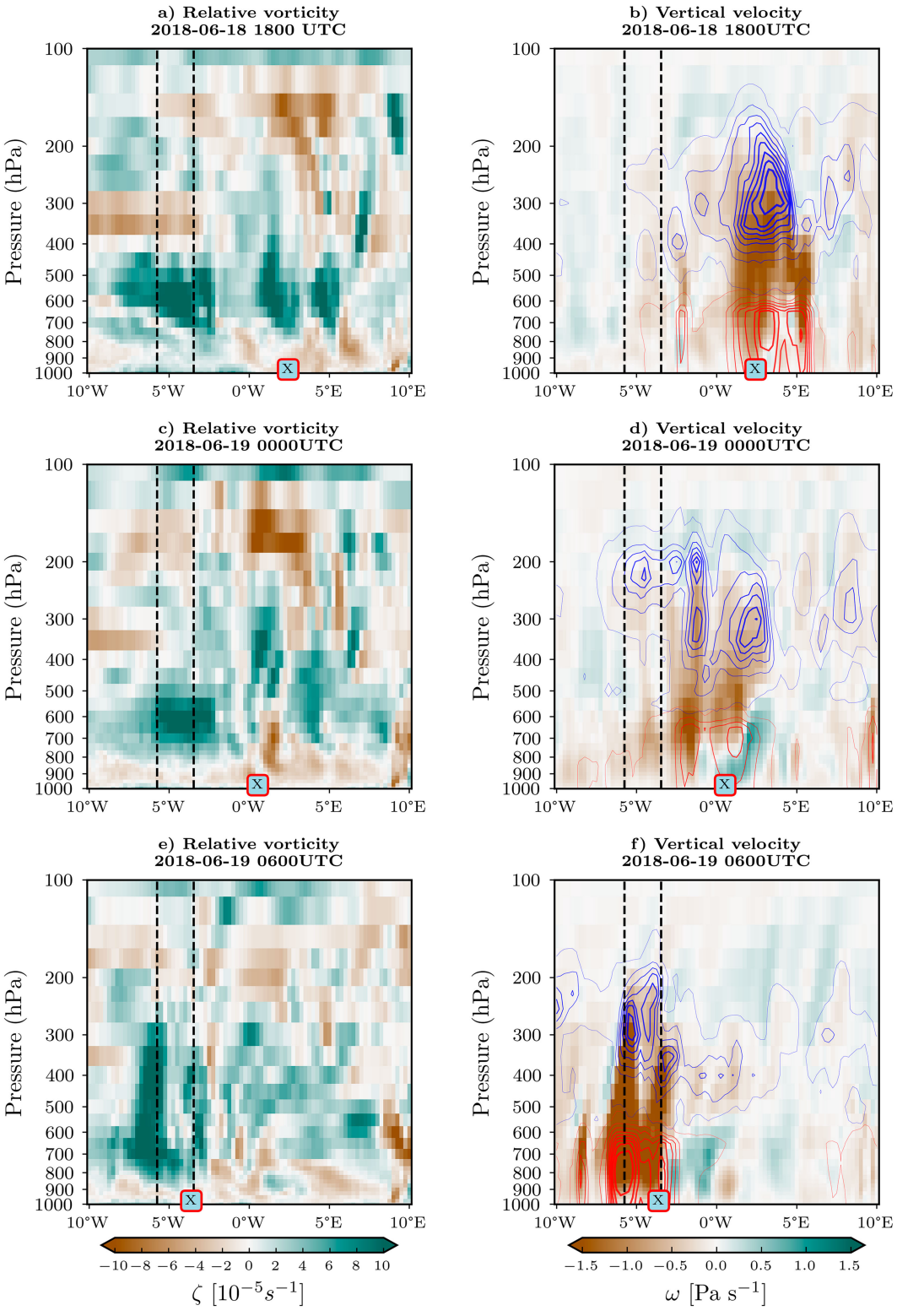

FIG. 11. Zonal cross sections of (left) relative vorticity and (right) vertical velocity shown as absolute values averaged over 4.25°–5.75°N latitude band on (top) 1800 UTC 18 Jun 2018, (center) 0000 UTC 19 Jun 2018, and (bottom) 0600 UTC 19 Jun 2018. The blue and red contours in the panels in the right column represent ice water (0.01–0.33, in 0.04 intervals) and rainwater (0.01–0.44, in 0.048 intervals) content (kg kg^{-1}), respectively. The x markers along the *x* axis show the positions of the MCS centroid at the respective time steps.

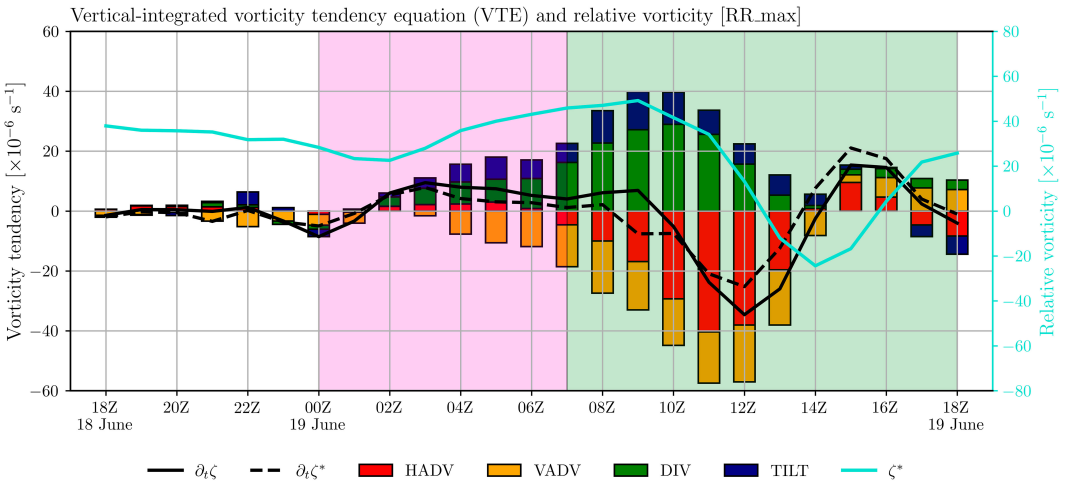

FIG. 12. Hourly contribution of VTE components HADV (red bars), VADV (yellow), DIV (green), and TILT (dark blue) to the change in relative vorticity ($\partial_t\zeta$, solid black line) from 1800 UTC 18 Jun to 1200 UTC 19 Jun. The light blue and dashed black curves represent the relative vorticity ζ^* and its hourly tendency ($\partial_t\zeta^*$), respectively, directly inferred from ERA5. All quantities are averaged on a 1° × 1° box centered around RR_max (i.e., 5.25°N, 5°W). The pink and green backgrounds highlight the periods during maximum rainfall in the RGs and ERA5, respectively.

intensification of the moist vortex. The pink and green backgrounds in Fig. 12 highlight the periods during extreme rainfall in observation and ERA5, respectively. Furthermore, the following quantities are shown as curves, all hourly based and vertically averaged within the 1000–600-hPa layers: 1) the net hourly tendency of relative vorticity ($\partial_t\zeta$, solid black line) derived from the VTE in Eq. (1) and 2) the relative vorticity (ζ^*, solid light blue) and 3) its net hourly tendency ($\partial_t\zeta^*$, dashed black line), both directly derived from the relative vorticity field in ERA5. The latter is plotted to test to what extent the VTE is capable of closing the budget.

Over the analysis domain, the buildup of the vortex occurred in a span of roughly 7 h between 0200 and 0900 UTC 19 June, where $\partial_t\zeta$ attains positive values. In the beginning, positive tendencies are generated by the TILT term (blue bars), which can be linked to the aforementioned presence of LLWS (see Fig. 10) as well as an inhomogeneous distribution of vertical motions that are likely associated with existing convective activity (e.g., Fig. 11d). However, we note that the tilting term might carry the largest uncertainty of all VTE components. While the convection parameterization reasonably captures the bulk effect of the MCS, it most likely underestimates the spatiotemporal variability of the vertical velocity field. Thus, the net tendency of the tilting term must be taken with caution. Increasing positive contributions to the vorticity budget is found for the DIV term (green bars) and eventually dominates by the time the relative vorticity reaches its maximum value at around 0900 UTC 19 June, which likely indicates a fully established vortex in the domain. Recalling the temporal evolution of ERA5 rainfall in Fig. 8d, the most intense rainfall in the study domain slightly lags the largest values of DIV, suggesting an important role of DIV in preconditioning the environmental setting for enhanced rainfall by increasing column moisture content. Indicative for vortex stretching within enhanced updrafts, this stage is most likely associated with the passage of the MCS. At the same time, it is counterbalanced and subsequently overcompensated by the advection terms HADV and VADV, the former of which suggests the advection of less cyclonic vorticity into the area of the vortex center and, eventually, its departure out of the study domain. Given the localized, small-scale effects an MCS can have, we emphasize that by using a global reanalysis dataset, the VTE might not entirely capture the effects of small-scale vorticity sources and sinks. However, the vorticity budget $\partial_t\zeta$ based on the VTE and the budget directly inferred from the ERA5 catalogue $\partial_t\zeta^*$ overall align well in their temporal evolution, providing confidence in the calculated VTE in describing the changes in relative vorticity for this case. In summary, this analysis does not entirely explain the intricate mesoscale dynamical reasons that facilitated the extreme event but rather underscores the relevance of an intensified vortex, for trapping and enhancing moisture levels which can positively feedback in efficient rainfall production within the MCS. While the importance of vortex stretching for the reinforcement of the vortex supports presumptions made in the respective rainfall cases in Maranan et al. (2019) and Beucher et al. (2020), extreme precipitation appears to be possible even with a weakening of the MCS in the present case.

d. Forecast challenges of the extreme rainfall event and moist vortex

To assess the level of practical predictability of this case, the EFI (see section 2f) and, in addition, SOT based on the ECMWF ensemble prediction system are simple, yet effective, indicators of how well and how strong extreme weather is forecasted as a function of lead time. In Fig. 13, both EFI (shaded) and SOT (colored contours) are shown for 12-hourly ECMWF forecasts up to 5 days (D-5) prior initialized at 1200 UTC to the verification date and time of the extreme event, which is set to 0000 UTC 19 June 2018, for the sake of

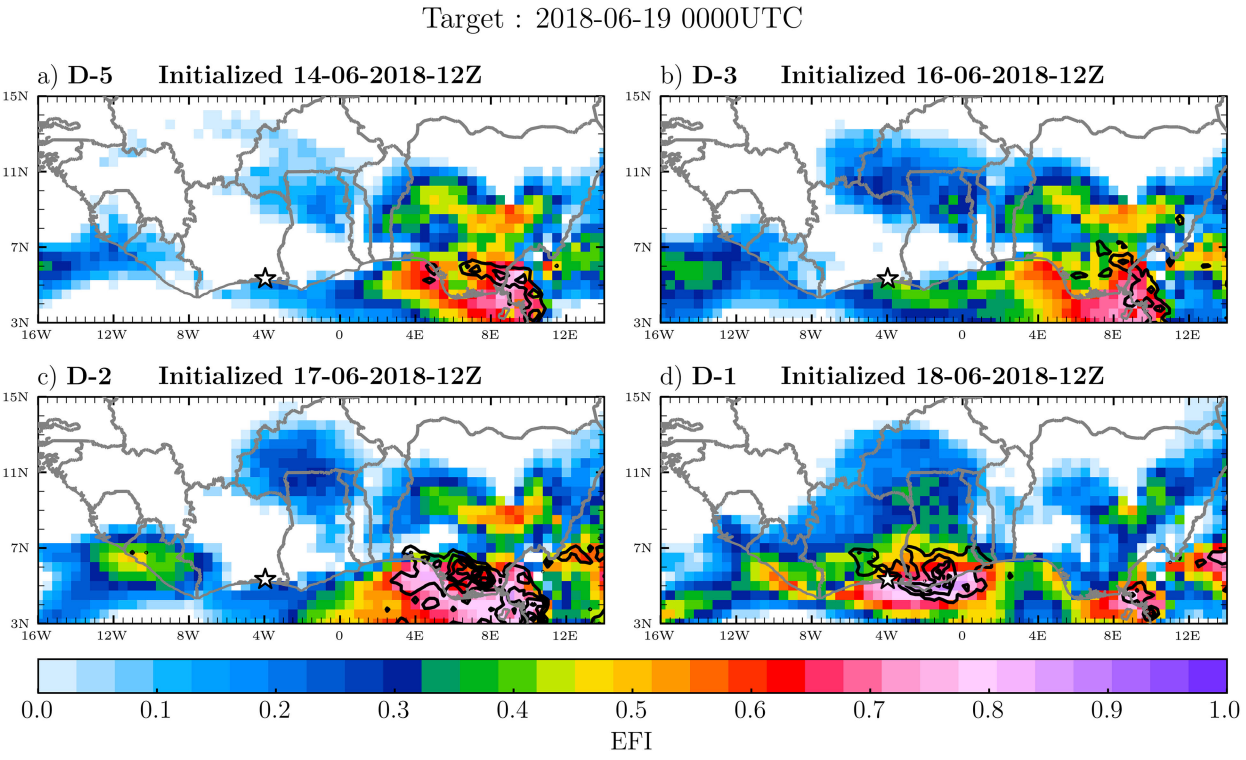

FIG. 13. ECMWF-EPS-based EFI (shaded) and SOT (contours) regarding 24-h precipitation for the verification date at 0000 UTC 19 Jun 2018, initialized at 1200 UTC at different lead times: (a) D-5, (b) D-3, (c) D-2, and (d) D-1 prior to the verification date, i.e., around the onset of the extreme rainfall event. The black-outlined star marker indicates the District of Abidjan.

simplicity. Over the District of Abidjan region (black star), hardly any indication of extreme rainfall and no evident changes in the spatial pattern of EFI are seen in the period between D-5 and 2 days (D-2) (Figs. 13a–c). Enhanced and persistent EFI (>0.5) and SOT (>1) are confined over the Bight of Bonny and the Cameroon Mountains where the MCS was initiated. This suggests that ENS never predicted the long-lasting westward translation of the MCS along the Guinea Coast region. A major shift in the EFI pattern is not seen until 1 day (D-1) at 1200 UTC 18 June 2018, i.e., 12 h prior to the event (Fig. 13d). Here, the area of enhanced EFI and SOT has considerably shifted to the west and is now located over the coastal area of Ghana and parts of the District of Abidjan region. This suggests that the approach of the mature MCS and its dynamical signatures were eventually captured in the D-1 forecast.

Insights into the PW and mass-weighted low-level wind fields for the verification date as predicted by the ECMWF deterministic forecast are presented in Fig. 14 at initialization points D-5, 3 days (D-3), and D-1 at 1200 UTC. Note that the verification date and time is 6 h later at 0600 UTC 19 June 2018, to account for the delayed onset of heavy ERA5 rainfall in the District of Abidjan region compared to observation (see Fig. 8b). As a reference, Fig. 14d depicts the situation in ERA5 again like in Fig. 10f, showing the well-developed moist vortex over the District of Abidjan domain. Evidently, none of the forecasts exhibits a vortex structure over the District of Abidjan on the verification date (Figs. 14a–c), which is in line with the lack of enhanced EFI values in Fig. 13. Moreover, it becomes apparent how influential the presence of the vortex on the large-scale flow is. While a regionwide cyclonic "inflow" toward the vortex center is identified in ERA5, even with northerlies manifesting to the northwest (Fig. 14d), the District of Abidjan region and the Guinea Coast are generally dominated by southerlies and southwesterlies in all forecast runs. However, with the lack of a vortex in the low-level flow, the enhanced PW is likely mostly a consequence of the assimilated MCS signature, as alluded above. In conclusion, the source of predictability of this extreme rainfall case in the District of Abidjan region might be more linked to the presence and position of the MCS alone in the forecasts rather than the development of a moist vortex. However, it is likely the latter, or more precisely the interaction between the MCS and the vortex, that likely carries predictive power for extreme events. In this case study, the forecasts failed to capture it.

4. Summary and conclusions

This manuscript investigated the (thermo)dynamical drivers and settings behind the flood-inducing extreme rainfall event along the Guinea Coast, which produced one of the highest recorded daily rainfall amounts at the Cocody station in the District of Abidjan with 302 mm on 18–19 June 2018.

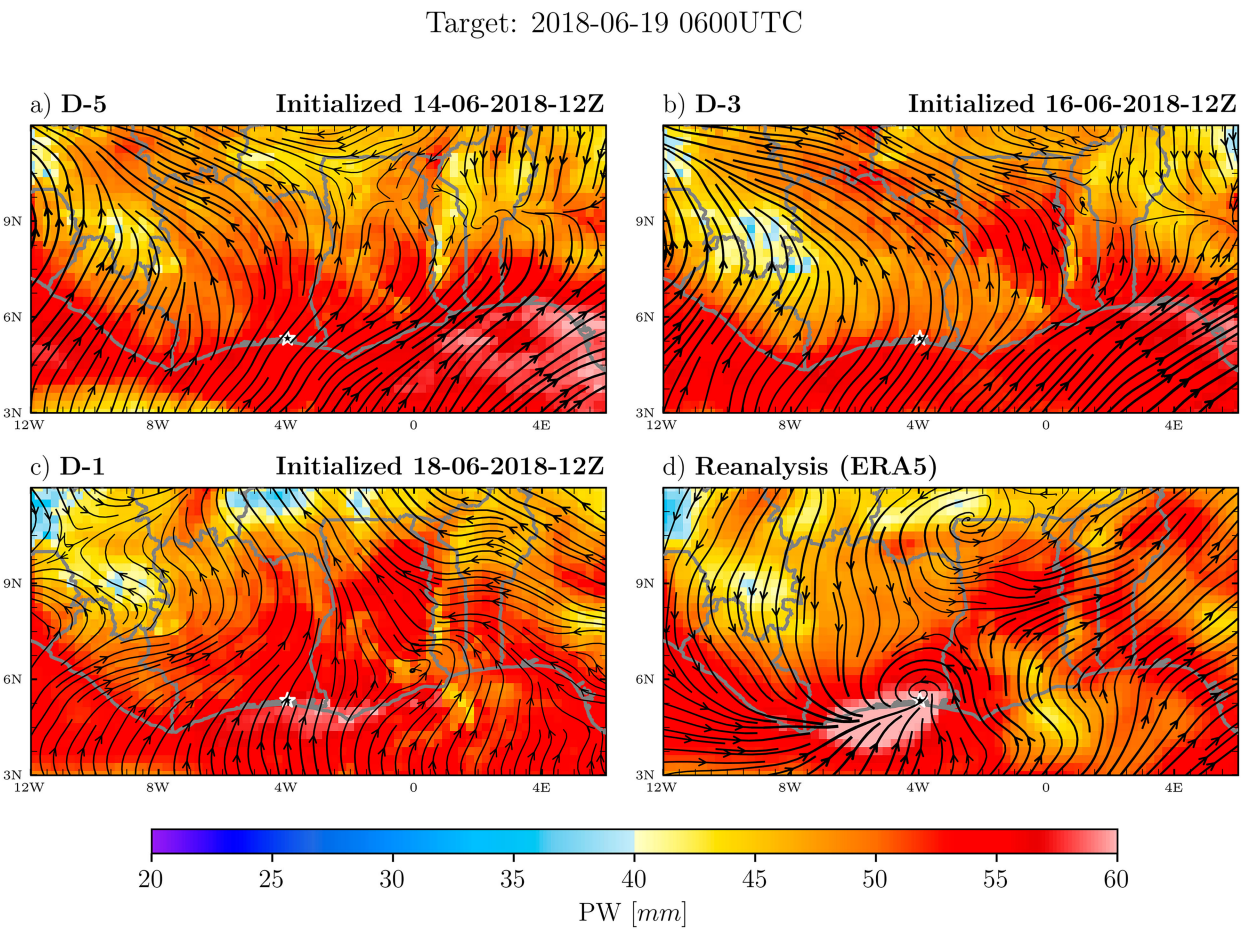

FIG. 14. As in Fig. 10 (middle), but for ECMWF deterministic forecasts at lead times (a) D-5, (b) D-3, and (c) D-1, prior to the verification date on 0600 UTC 19 Jun 2018. (d) The ERA5 field on the verification date is shown. The white star marker indicates the District of Abidjan.

During the event, many other surrounding stations also exceeded 100 mm within 24 h, which led to severe urban floods and considerable economical and human losses (PDNA 2019; Coulibaly et al. 2024). Leveraging a unique set of station-based daily and hourly rainfall data from SODEXAM, KASS-D, and the EVIDENCE project (Zahiri et al. 2023), the onset and evolution of the extreme event were evaluated and eventually compared with the widely used IMERG product. By further using fields in ERA5, cloud features in IR imagery of SEVIRI and MW-based brightness temperatures, as well as ECMWF ensemble and deterministic forecasts, the rainfall systems and environmental settings that were linked to the extreme event were analyzed with a particular focus on the period between 1800 UTC 18 June 2018 and 0600 UTC 19 June 2018, corresponding to the (pre)onset stage of the intense rainfall over the District of Abidjan. The following results stand out:

- The recorded 302 mm at the Cocody station was the second highest daily rainfall amount in the Abidjan area in available data records dating back to 1936. In the extensive KASS-D database, daily rainfall amounts over 300 mm are found exclusively along the coast of Côte d'Ivoire, whereas 150–200 mm can be regarded as extreme farther inland and 200–250 mm can be regarded as across other stations at the Guinea Coast.
- The major rainfall system associated with the extreme event was a long-lasting MCS which originated over the Cameroon Highlands and propagated westward along the Guinea Coast region. A striking aspect is that rainfall was extreme despite the weakening of the MCS (according to IR and MW imagery) as it arrived over the District of Abidjan area.
- Despite IMERG and ERA5 showing a delayed onset and considerable underestimation of the event rainfall compared to rain gauge observations, and considerably underestimating the event rainfall, it confirms the extreme nature of the event by exhibiting values well beyond the 99th percentile regarding the accumulated 12-h rainfall, i.e., roughly the duration of the event over the course of the night of 19 June 2018.
- The manifestation of an intense and deep moist vortex over the District of Abidjan was linked to exceptionally strong and high tropospheric moisture content and convergence. The vorticity equation analysis indicates a considerable

contribution from the tilting and divergence term to the local cyclonic vorticity tendency, where the divergence term gradually dominates toward the peak intensity of the vortex. This supports the hypothesis of an active MCS–vortex interaction during the extreme event.
- A high probability for extreme rainfall over the District of Abidjan was not predicted by the ensemble prediction system of the ECMWF until 12 h before the event onset. A forecast shift to high EFI (>0.8) over the District of Abidjan was likely a consequence of the assimilation of the signatures of the MCS, which was located closer to the District of Abidjan than any of the previous forecasts had predicted. Moreover, none of the deterministic forecasts exhibited an accompanying low-level moist vortex.

First of all, the question on whether ERA5 reasonably captured the extreme event represented by model-sensitive parameters like vertical motion, moisture convergence, and precipitation, which emanate from ECMWF (re)analyses and short-term forecasts (Hersbach et al. 2020), respectively, was addressed throughout the study. All the abovementioned parameters are not observed and thus not assimilated. While—not surprisingly—ERA5 rainfall underestimates absolute rainfall totals of the extreme event at the investigated tropical latitude (e.g., Lavers et al. 2022), a percentile-based view with respect to its model climate indicates that ERA5 indeed captured the extreme rainfall over Abidjan. This is supported by the fact that the investigated MCS is present in synthetic satellite images of the short-term IFS forecast over various initial times (see Fig. S4). However, most likely due to limitations of the underlying convection parameterization in the IFS model, the timing as well as the intensity of extreme rainfall compared to rain gauge and IMERG observations over Abidjan is misrepresented, and the strongest rainfall occurred to the southwest of the District of Abidjan in ERA5. This led to the decision to spatially shift the analysis to this domain of strongest ERA5 rainfall to facilitate a process-oriented analysis on the generation of extreme rainfall in the present case study. Yet, largest uncertainties pertain to, for example, the tilting term in the VTE since it contains vertical motion taken from a parameterized model. Eventually, it remains to be seen whether future iterations of the ECMWF reanalysis with an updated IFS moist physics scheme (Bechtold et al. 2020) can mitigate some of the deficiencies in the present extreme rainfall case.

Complementing the works of, e.g., Engel et al. (2017), Maranan et al. (2019), Lafore et al. (2017), and Beucher et al. (2020), the present extreme rainfall case supports the coexistence between MCSs and moist vortex as an important aspect for facilitating West African precipitation extremes. From the above-referenced case studies in the Sahel and Guinea coastal climate zones, the moist vortices appear to be instrumental for (i) the extremes in the preevent moisture convergence and columnar water vapor content, (ii) a swift moisture recharging to allow for sequences of MCS within less than 12 h (Engel et al. 2017) or extreme rainfall intensities lasting several hours like in the present case, and (iii) a slow propagation speed of the MCSs. However, a novel insight to the previous case studies is the fact that the most extreme coastal precipitation does not require the deepest and most intense (based on satellite radiances) convective systems as long as abundant moisture is effectively converted to rainfall, i.e., widespread and long-lasting convection associated with moist vortices. Overall, like Tomassini et al. (2017), Maranan et al. (2019), and Beucher et al. (2020), the present study indicates that such vortices may be formed or intensified by an interaction between the MCS and the environmental flow. Knippertz et al. (2017) and Vondou et al. (2026) describe cyclone–anticyclone couplets over the Gulf of Guinea whose dynamic origin is also unclear—none of them could be related to tropical waves. Given their importance for extreme rainfall and tropospheric aerosol content (Knippertz et al. 2017), research into their origin and climatology is urgently needed. This also pertains to the question as to how often such coastal vortices are related to relatively weak convective systems as also described in Hamada et al. (2015) and Xu et al. (2022).

Given the low predictability of current NWP models to forecast 24-h rainfall totals of the next days, as extensively documented in Vogel et al. (2018, 2020) and Walz et al. (2021), the low short-range predictability of the present case does not come as a surprise. However, Kniffka et al. (2020) showed indications of improved predictability of rainfall within NWP models when a synoptic forcing was present. In this context, our results suggest that once the coastal MCS was well established and potentially reflected in assimilated wind information about 12 h before the event, the model was able to indicate that an extreme event was imminent. In this regard, it needs to be underlined that the predictive skill of the IFS to forecast the longevity of the MCS is likely hampered by the limitations of the convection parameterization scheme. General improvements in predicting such events could be expected by forecasts with convection-permitting models (e.g., Hanley et al. 2021; Mittermaier et al. 2022). However, based on three West African monsoon seasons, F. Rein et al. (2025, personal communication) show in their thorough study on the skill of 24-h precipitation forecast of various forecasting approaches (e.g., deterministic vs ensemble, parameterized vs explicit) that models with an explicit treatment of convection outperform parameterized models only at very few grid points over West and central Africa. Therefore, future studies should further examine sources of enhanced predictive skill of rainfall, also using promising statistical and artificial intelligence approaches which also use forecast of wave disturbances as predictors (e.g., Vogel et al. 2021; Rasheeda Satheesh et al. 2023; Walz et al. 2024) to allow for actionable early warning forecast information. Such information is urgently needed since the growing megacities along the Guinea Coast will likely be exposed to even more extreme 24-h rainfall totals in the coming decades.

Acknowledgments. We thank the three anonymous reviewers for their time spent on the manuscript and the insightful comments on the manuscript which helped to improve it considerably. The authors acknowledge funding from the German Federal Ministry of Education and Research

(BMBF) through the WASCAL Research Action Plan 2.0 (WRAP2.0) FURIFLOOD project (Current and future risks of urban and rural flooding in West Africa–An integrated analysis and eco-system-based solutions; Grants 01LG2081A and 01LG2086A). The second and third authors also receive funding from the BMBF project German Academic Network for Capacity Development in Climate Change Adaptations in Africa (NetCDA; Grant 01LG2301E). The authors further acknowledge the EVIDENCE Project for providing a part of the dataset used in the framework of this research. They finally thank FURIFLOOD partners for their support.

Data availability statement. ERA5 data were downloaded from the European Centre for Medium-Range Weather Forecasts (ECMWF) and the Copernicus Climate Change Service (C3S) at the Climate Data Store (https://cds.climate.copernicus.eu/) (Hersbach et al. 2020). The EFI and SOT were downloaded from the MARS archive available from https://www.ecmwf.int/en/elibrary/80518-mars-ecmwf-meteorological-archive. The Spinning Enhanced Visible and Infrared Imager (SEVIRI) was downloaded from the European Organisation for the Exploitation of Meteorological Satellites (https://user.eumetsat.int/). GPM-IMERG rainfall version 7 data used in this study are available at https://daac.gsfc.nasa.gov/datasets/ (Huffman et al. 2020). The convective-system-tracked database is available from https://doi.org/10.5281/zenodo.4244985 (Feng et al. 2021). Code for the main figures of this study is available from the GitHub repository at https://github.com/ibrahimsalifou/Paper-MCS.

REFERENCES

Abiodun, B. J., J. Adegoke, A. A. Abatan, C. A. Ibe, T. S. Egbebiyi, F. Engelbrecht, and I. Pinto, 2017: Potential impacts of climate change on extreme precipitation over four African coastal cities. *Climatic Change*, **143**, 399–413, https://doi.org/10.1007/s10584-017-2001-5.

Ageet, S., A. H. Fink, M. Maranan, J. E. Diem, J. Hartter, A. L. Ssali, and P. Ayabagabo, 2022: Validation of satellite rainfall estimates over equatorial East Africa. *J. Hydrometeor.*, **23**, 129–151, https://doi.org/10.1175/JHM-D-21-0145.1.

Aminou, D. M. A., 2002: MSG's SEVIRI instrument. *ESA Bull.*, **11**, 15–17.

Amouin, J., K. Y. Kouadio, M. Kacou, S. Djakouré, and S. Ta, 2021: Diagnosis of the causes of the rain flooding in June in the West Africa coastal area. *Atmos. Climate Sci.*, **11**, 11–31, https://doi.org/10.4236/acs.2021.111002.

Arkin, P. A., 1979: The relationship between fractional coverage of high cloud and rainfall accumulations during GATE over the B-scale array. *Mon. Wea. Rev.*, **107**, 1382–1387, https://doi.org/10.1175/1520-0493(1979)107<1382:TRBFCO>2.0.CO;2.

Atiah, W. A., L. K. Amekudzi, and S. K. Danuor, 2023: Mesoscale convective systems and contributions to flood cases in Southern West Africa (SWA): A systematic review. *Wea. Climate Extremes*, **39**, 100551, https://doi.org/10.1016/j.wace.2023.100551.

Attoumane, A., S. Dos Santos, M. Kacou, A. D. André, A. W. Karamoko, L. Seguis, and E.-P. Zahiri, 2022: Individual perceptions on rainfall variations versus precipitation trends from satellite data: An interdisciplinary approach in two socio-economically and topographically contrasted districts in Abidjan, Côte d'ivoire. *Int. J. Disaster Risk Reduct.*, **81**, 103285, https://doi.org/10.1016/j.ijdrr.2022.103285.

Baidu, M., J. Schwendike, J. H. Marsham, and C. Bain, 2022: Effects of vertical wind shear on intensities of mesoscale convective systems over West and Central Africa. *Atmos. Sci. Lett.*, **23**, e1094, https://doi.org/10.1002/asl.1094.

Bechtold, P., N. Semane, P. Lopez, J.-P. Chaboureau, A. Beljaars, and N. Bormann, 2014: Representing equilibrium and nonequilibrium convection in large-scale models. *J. Atmos. Sci.*, **71**, 734–753, https://doi.org/10.1175/JAS-D-13-0163.1.

——, R. Forbes, I. Sandu, S. Lang, and M. Ahlgrimm, 2020: A major moist physics upgrade for the IFS. *ECMWF Newsletter*, No. 164, ECMWF, Reading, United Kingdom, 24–32, https://www.ecmwf.int/en/elibrary/81181-major-moist-physics-upgrade-ifs.

Berry, G. J., and C. Thorncroft, 2005: Case study of an intense African easterly wave. *Mon. Wea. Rev.*, **133**, 752–766, https://doi.org/10.1175/MWR2884.1.

Beucher, F., J.-P. Lafore, and N. Chapelon, 2020: Simulation and analysis of the moist vortex associated with the extreme rain event of Ouagadougou in 2009. *Quart. J. Roy. Meteor. Soc.*, **146**, 86–104, https://doi.org/10.1002/qj.3645.

Bickle, M. E., J. H. Marsham, A. N. Ross, D. P. Rowell, D. J. Parker, and C. M. Taylor, 2021: Understanding mechanisms for trends in Sahelian squall lines: Roles of thermodynamics and shear. *Quart. J. Roy. Meteor. Soc.*, **147**, 983–1006, https://doi.org/10.1002/qj.3955.

Boisserie, M., L. Descamps, and P. Arbogast, 2016: Calibrated forecasts of extreme windstorms using extreme forecast index (EFI) and shift of tails (SOT). *Wea. Forecasting*, **31**, 1573–1589, https://doi.org/10.1175/WAF-D-15-0027.1.

Burpee, R. W., 1972: The origin and structure of easterly waves in the lower troposphere of North Africa. *J. Atmos. Sci.*, **29**, 77–90, https://doi.org/10.1175/1520-0469(1972)029<0077:TOASOE>2.0.CO;2.

Cornforth, R., and Coauthors, 2017: Synoptic systems. *Meteorology of Tropical West Africa: The Forecasters' Handbook*, D. J. Parker and M. Diop-Kane, Eds., Wiley, 40–89.

Coulibaly, K. A., P. A. Dibi-Anoh, B. N. J. Tah, H. Anoh, K. C. N'da, S. C. Ahilé, K. B. Djè, and D. Konaté, 2024: Occurrence of extreme rainfall and flood risks in Yopougon, Abidjan, Southeast Côte d'Ivoire from 1971 to 2022. *Amer. J. Climate Change*, **13**, 427–451, https://doi.org/10.4236/ajcc.2024.133020.

Diedhiou, S., M. Rauch, A. Lahat Dieng, J. Bliefernicht, S. Sy, S. M. Sall, and H. Kunstmann, 2024: Extreme rainfall in Dakar (Senegal): A case study for September 5, 2020. *Front. Water*, **6**, 1439404, https://doi.org/10.3389/frwa.2024.1439404.

Douglas, I., K. Alam, M. Maghenda, Y. McDonnell, L. McLean, and J. Campbell, 2008: Unjust waters: Climate change, flooding and the urban poor in Africa. *Environ. Urbanization*, **20**, 187–205, https://doi.org/10.1177/0956247808089156.

Draper, D. W., D. A. Newell, F. J. Wentz, S. Krimchansky, and G. M. Skofronick-Jackson, 2015: The Global Precipitation Measurement (GPM) Microwave Imager (GMI): Instrument overview and early on-orbit performance. *IEEE J. Sel. Top. Appl. Earth Obs. Remote Sens.*, **8**, 3452–3462, https://doi.org/10.1109/JSTARS.2015.2403303.

Engel, T., A. H. Fink, P. Knippertz, G. Pante, and J. Bliefernicht, 2017: Extreme precipitation in the West African cities of Dakar and Ouagadougou: Atmospheric dynamics and implications for flood risk assessments. *J. Hydrometeor.*, **18**, 2937–2957, https://doi.org/10.1175/JHM-D-16-0218.1.

Feng, Z., and Coauthors, 2021: A global high-resolution mesoscale convective system database using satellite-derived cloud tops, surface precipitation, and tracking. *J. Geophys. Res. Atmos.*, **126**, e2020JD034202, https://doi.org/10.1029/2020JD034202.

Fink, A. H., and A. Reiner, 2003: Spatiotemporal variability of the relation between African Easterly Waves and West African Squall Lines in 1998 and 1999. *J. Geophys. Res.*, **108**, 4332, https://doi.org/10.1029/2002JD002816.

——, D. G. Vincent, and V. Ermert, 2006: Rainfall types in the West African Sudanian zone during the summer monsoon 2002. *Mon. Wea. Rev.*, **134**, 2143–2164, https://doi.org/10.1175/MWR3182.1.

——, and Coauthors, 2017: Mean climate and seasonal cycle. *Meteorology of Tropical West Africa*, D. J. Parker, M. Diop-Kane, Eds., John Wiley and Sons Ltd., 1–39.

Fischer, C., A. H. Fink, E. Schömer, M. Rautenhaus, and M. Riemer, 2024: An objective identification technique for potential vorticity structures associated with African easterly waves. *Geosci. Model Dev.*, **17**, 4213–4228, https://doi.org/10.5194/gmd-17-4213-2024.

Fitzpatrick, R. G. J., and Coauthors, 2020: What drives the intensification of mesoscale convective systems over the West African Sahel under climate change? *J. Climate*, **33**, 3151–3172, https://doi.org/10.1175/JCLI-D-19-0380.1.

Haiden, T., M. J. Rodwell, D. S. Richardson, A. Okagaki, T. Robinson, and T. Hewson, 2012: Intercomparison of global model precipitation forecast skill in 2010/11 using the SEEPS score. *Mon. Wea. Rev.*, **140**, 2720–2733, https://doi.org/10.1175/MWR-D-11-00301.1.

Hamada, A., Y. N. Takayabu, C. Liu, and E. J. Zipser, 2015: Weak linkage between the heaviest rainfall and tallest storms. *Nat. Commun.*, **6**, 6213, https://doi.org/10.1038/ncomms7213.

Hanley, K. E., J. S. R. Pirret, C. L. Bain, A. J. Hartley, H. W. Lean, S. Webster, and B. J. Woodhams, 2021: Assessment of convection-permitting versions of the Unified Model over the Lake Victoria basin region. *Quart. J. Roy. Meteor. Soc.*, **147**, 1642–1660, https://doi.org/10.1002/qj.3988.

Hastings, D. A., P. K. Dunbar, and A. M. Hittelman, 2000: Assessing the global land one-km base elsevation DEM. *Geodesy Beyond 2000*, K.-P. Schwarz, Ed., International Association of Geodesy Symposia, Vol. 121, Springer, 101–106, https://doi.org/10.1007/978-3-642-59742-8_16.

Hersbach, H., and Coauthors, 2020: The ERA5 global reanalysis. *Quart. J. Roy. Meteor. Soc.*, **146**, 1999–2049, https://doi.org/10.1002/qj.3803.

Holton, J. R., and G. J. Hakim, 2013: *An Introduction to Dynamic Meteorology*. Vol. 88. Academic Press, 532 pp.

Hou, A. Y., and Coauthors, 2014: The Global Precipitation Measurement mission. *Bull. Amer. Meteor. Soc.*, **95**, 701–722, https://doi.org/10.1175/BAMS-D-13-00164.1.

Huffman, G. J., and Coauthors, 2007: The TRMM Multisatellite Precipitation Analysis (TMPA): Quasi-global, multiyear, combined-sensor precipitation estimates at fine scales. *J. Hydrometeor.*, **8**, 38–55, https://doi.org/10.1175/JHM560.1.

——, and Coauthors, 2020: Integrated Multi-satellite Retrievals for the Global Precipitation Measurement (GPM) Mission (IMERG). *Satellite Precipitation Measurement*, V. Levizzani et al., Eds., Advances in Global Change Research, Vol. 1, Springer International Publishing, 343–353.

——, R. F. Adler, A. Behrangi, D. T. Bolvin, E. J. Nelkin, G. Gu, and M. R. Ehsani, 2023: The new version 3.2 Global Precipitation Climatology Project (GPCP) monthly and daily precipitation products. *J. Climate*, **36**, 7635–7655, https://doi.org/10.1175/JCLI-D-23-0123.1.

IPCC, 2022: *Climate Change 2022: Impacts, Adaptation and Vulnerability*. 1st ed. H.-O. Pörtner et al., Eds., Cambridge University Press, 3056 pp.

Janiga, M. A., and C. D. Thorncroft, 2016: The influence of African easterly waves on convection over tropical Africa and the East Atlantic. *Mon. Wea. Rev.*, **144**, 171–192, https://doi.org/10.1175/MWR-D-14-00419.1.

Janowiak, J. E., R. J. Joyce, and Y. Yarosh, 2001: A real-time global half-hourly pixel-resolution infrared dataset and its applications. *Bull. Amer. Meteor. Soc.*, **82**, 205–218, https://doi.org/10.1175/1520-0477(2001)082<0205:ARTGHH>2.3.CO;2.

Kendon, E. J., R. A. Stratton, S. Tucker, J. H. Marsham, S. Berthou, D. P. Rowell, and C. A. Senior, 2019: Enhanced future changes in wet and dry extremes over Africa at convection-permitting scale. *Nat. Commun.*, **10**, 1794, https://doi.org/10.1038/s41467-019-09776-9.

Klein, C., and C. M. Taylor, 2020: Dry soils can intensify mesoscale convective systems. *Proc. Natl. Acad. Sci. USA*, **117**, 21 132–21 137, https://doi.org/10.1073/pnas.2007998117.

——, F. Nkrumah, C. M. Taylor, and E. A. Adefisan, 2021: Seasonality and trends of drivers of mesoscale convective systems in southern West Africa. *J. Climate*, **34**, 71–87, https://doi.org/10.1175/JCLI-D-20-0194.1.

Kniffka, A., and Coauthors, 2020: An evaluation of operational and research weather forecasts for southern West Africa using observations from the DACCIWA field campaign in June–July 2016. *Quart. J. Roy. Meteor. Soc.*, **146**, 1121–1148, https://doi.org/10.1002/qj.3729.

Knippertz, P., and Coauthors, 2017: A meteorological and chemical overview of the DACCIWA field campaign in West Africa in June–July 2016. *Atmos. Chem. Phys.*, **17**, 10 893–10 918, https://doi.org/10.5194/acp-17-10893-2017.

Konate, L., B. H. Kouadio, B. K. Djè, G. E. Ake, N. B. V. Hermann, L. Gnagne, E. K. Kouame, and J. Biemi, 2016: Heavy daily rainfall characterization and flooding repeating: Contribution of three (3) days sliding total to the purposefulness of threshold amount rainfall inducing flooding (Abidjan district, south-east of Ivory Coast). *Int. J. Innov. Appl. Stud.*, **17**, 990–1003.

Kreibich, H., and Coauthors, 2022: The challenge of unprecedented floods and droughts in risk management. *Nature*, **608**, 80–86, https://doi.org/10.1038/s41586-022-04917-5.

Lafore, J.-P., and Coauthors, 2017: A multi-scale analysis of the extreme rain event of Ouagadougou in 2009. *Quart. J. Roy. Meteor. Soc.*, **143**, 3094–3109, https://doi.org/10.1002/qj.3165.

Lalaurette, F., 2003: Early detection of abnormal weather conditions using a probabilistic extreme forecast index. *Quart. J. Roy. Meteor. Soc.*, **129**, 3037–3057, https://doi.org/10.1256/qj.02.152.

Lavers, D. A., F. Pappenberger, and E. Zsoter, 2014: Extending medium-range predictability of extreme hydrological events in Europe. *Nat. Commun.*, **5**, 5382, https://doi.org/10.1038/ncomms6382.

——, A. Simmons, F. Vamborg, and M. J. Rodwell, 2022: An evaluation of ERA5 precipitation for climate monitoring. *Quart. J. Roy. Meteor. Soc.*, **148**, 3152–3165, https://doi.org/10.1002/qj.4351.

Magnusson, L., and Coauthors, 2019: ECMWF activities for improved hurricane forecasts. *Bull. Amer. Meteor. Soc.*, **100**, 445–458, https://doi.org/10.1175/BAMS-D-18-0044.1.

Maranan, M., A. H. Fink, and P. Knippertz, 2018: Rainfall types over southern West Africa: Objective identification, climatology and synoptic environment. *Quart. J. Roy. Meteor. Soc.*, **144**, 1628–1648, https://doi.org/10.1002/qj.3345.

——, ——, ——, S. D. Francis, A. B. Akpo, G. Jegede, and C. Yorke, 2019: Interactions between convection and a moist vortex associated with an extreme rainfall event over southern West Africa. *Mon. Wea. Rev.*, **147**, 2309–2328, https://doi.org/10.1175/MWR-D-18-0396.1.

——, ——, ——, L. K. Amekudzi, W. A. Atiah, and M. Stengel, 2020: A Process-based validation of GPM IMERG and its sources using a mesoscale rain gauge network in the West African forest zone. *J. Hydrometeor.*, **21**, 729–749, https://doi.org/10.1175/JHM-D-19-0257.1.

Mathon, V., and H. Laurent, 2001: Life cycle of Sahelian mesoscale convective cloud systems. *Quart. J. Roy. Meteor. Soc.*, **127**, 377–406, https://doi.org/10.1002/qj.49712757208.

——, ——, and T. Lebel, 2002: Mesoscale convective system rainfall in the Sahel. *J. Appl. Meteor.*, **41**, 1081–1092, https://doi.org/10.1175/1520-0450(2002)041<1081:MCSRIT>2.0.CO;2.

Mittermaier, M., S. Landman, G. Csima, and S. Goodman, 2022: Convective-scale numerical weather prediction and warnings over Lake Victoria: Part II—Can model output support severe weather warning decision-making? *Meteor. Appl.*, **29**, e2055, https://doi.org/10.1002/met.2055.

Mohr, K. I., and C. D. Thorncroft, 2006: Intense convective systems in West Africa and their relationship to the African easterly jet. *Quart. J. Roy. Meteor. Soc.*, **132**, 163–176, https://doi.org/10.1256/qj.05.55.

Muller, B. M., H. E. Fuelberg, and X. Xiang, 1994: Simulations of the effects of water vapor, cloud liquid water, and ice on AMSU moisture channel brightness temperatures. *J. Appl. Meteor.*, **33**, 1133–1154, https://doi.org/10.1175/1520-0450(1994)033<1133:SOTEOW>2.0.CO;2.

Nicholson, S. E., 2013: The West African Sahel: A review of recent studies on the rainfall regime and its interannual variability. *Int. Scholarly Res. Not.*, **2013**, 453521, https://doi.org/10.1155/2013/453521.

——, C. Funk, and A. H. Fink, 2018: Rainfall over the African continent from the 19th through the 21st century. *Global Planet. Change*, **165**, 114–127, https://doi.org/10.1016/j.gloplacha.2017.12.014.

Nkrumah, F., T. Vischel, G. Panthou, N. A. B. Klutse, D. C. Adukpo, and A. Diedhiou, 2019: Recent trends in the daily rainfall regime in Southern West Africa. *Atmosphere*, **10**, 741, https://doi.org/10.3390/atmos10120741.

Osei, M. A., and Coauthors, 2023: Environment of severe storm formations over West Africa on the 26–28 June 2018. *Meteor. Appl.*, **30**, e2109, https://doi.org/10.1002/met.2109.

Panthou, G., T. Vischel, and T. Lebel, 2014: Recent trends in the regime of extreme rainfall in the Central Sahel. *Int. J. Climatol.*, **34**, 3998–4006, https://doi.org/10.1002/joc.3984.

Pantillon, F., P. Knippertz, and U. Corsmeier, 2017: Revisiting the synoptic-scale predictability of severe European winter storms using ECMWF ensemble reforecasts. *Nat. Hazards Earth Syst. Sci.*, **17**, 1795–1810, https://doi.org/10.5194/nhess-17-1795-2017.

PDNA, 2019: Evaluation des pertes, dommages et besoins suite aux inondations de juin 2018 à Abidjan. 220 pp., https://reporterre.net/IMG/pdf/rapportcatastrophesnaturellescotedivoire.pdf.

Peters, M., and G. Tetzlaff, 1988: The structure of West African Squall Lines and their environmental moisture budget. *Meteor. Atmos. Phys.*, **39**, 74–84, https://doi.org/10.1007/BF01041933.

Rasheeda Satheesh, A., P. Knippertz, A. H. Fink, E.-M. Walz, and T. Gneiting, 2023: Sources of predictability of synoptic-scale rainfall during the West African summer monsoon. *Quart. J. Roy. Meteor. Soc.*, **149**, 3721–3737, https://doi.org/10.1002/qj.4581.

Raynaud, L., B. Touzé, and P. Arbogast, 2018: Detection of severe weather events in a high-resolution ensemble prediction system using the Extreme Forecast Index (EFI) and Shift of Tails (SOT). *Wea. Forecasting*, **33**, 901–908, https://doi.org/10.1175/WAF-D-17-0183.1.

Recensement Général de la Population et de l'Habitat, 2022: Recensement général de la population et de l'habitat 2021: Resultats Globaux Definitifs. 37 pp., https://www.plan.gouv.ci/assets/fichier/RGPH2021-RESULTATS-GLOBAUX-VF.pdf.

Redelsperger, J.-L., A. Diongue, A. Diedhiou, J.-P. Ceron, M. Diop, J.-F. Gueremy, and J.-P. Lafore, 2002: Multi-scale description of a Sahelian synoptic weather system representative of the West African monsoon. *Quart. J. Roy. Meteor. Soc.*, **128**, 1229–1257, https://doi.org/10.1256/003590002320373274.

Redl, R., A. H. Fink, and P. Knippertz, 2015: An objective detection method for convective cold pool events and its application to northern Africa. *Mon. Wea. Rev.*, **143**, 5055–5072, https://doi.org/10.1175/MWR-D-15-0223.1.

Reed, R. J., D. C. Norquist, and E. E. Recker, 1977: The structure and properties of African wave disturbances as observed during phase III of GATE. *Mon. Wea. Rev.*, **105**, 317–333, https://doi.org/10.1175/1520-0493(1977)105<0317:TSAPOA>2.0.CO;2.

Rowell, D. P., and J. R. Milford, 1993: On the generation of African squall lines. *J. Climate*, **6**, 1181–1193, https://doi.org/10.1175/1520-0442(1993)006<1181:OTGOAS>2.0.CO;2.

Sanogo, S., A. H. Fink, J. A. Omotosho, A. Ba, R. Redl, and V. Ermert, 2015: Spatio-temporal characteristics of the recent rainfall recovery in West Africa. *Int. J. Climatol.*, **35**, 4589–4605, https://doi.org/10.1002/joc.4309.

Skofronick-Jackson, G., and Coauthors, 2017: The Global Precipitation Measurement (GPM) mission for science and society. *Bull. Amer. Meteor. Soc.*, **98**, 1679–1695, https://doi.org/10.1175/BAMS-D-15-00306.1.

Smith, R. K., 1983: *Lectures on Dynamical Meteorology*. Monash University, 159 pp.

Sultan, B., S. Janicot, and A. Diedhiou, 2003: The West African monsoon dynamics. Part I: Documentation of intraseasonal variability. *J. Climate*, **16**, 3389–3406, https://doi.org/10.1175/1520-0442(2003)016<3389:TWAMDP>2.0.CO;2.

Tan, J., G. J. Huffman, D. T. Bolvin, and E. J. Nelkin, 2019: IMERG V06: Changes to the morphing algorithm. *J. Atmos. Oceanic Technol.*, **36**, 2471–2482, https://doi.org/10.1175/JTECH-D-19-0114.1.

Taylor, C. M., and Coauthors, 2017: Frequency of extreme Sahelian storms tripled since 1982 in satellite observations. *Nature*, **544**, 475–478, https://doi.org/10.1038/nature22069.

Thorncroft, C. D., H. Nguyen, C. Zhang, and P. Peyrillé, 2011: Annual cycle of the West African monsoon: Regional circulations and associated water vapour transport. *Quart. J. Roy. Meteor. Soc.*, **137**, 129–147, https://doi.org/10.1002/qj.728.

Tomassini, L., D. J. Parker, A. Stirling, C. Bain, C. Senior, and S. Milton, 2017: The interaction between moist diabatic processes and the atmospheric circulation in African Easterly

Wave propagation. *Quart. J. Roy. Meteor. Soc.*, **143**, 3207–3227, https://doi.org/10.1002/qj.3173.

Tory, K. J., J. D. Kepert, J. A. Sippel, and C. M. Nguyen, 2012: On the use of potential vorticity tendency equations for diagnosing atmospheric dynamics in numerical models. *J. Atmos. Sci.*, **69**, 942–960, https://doi.org/10.1175/JAS-D-10-05005.1.

Tsonevsky, I., C. A. Doswell III, and H. E. Brooks, 2018: Early warnings of severe convection using the ECMWF extreme forecast index. *Wea. Forecasting*, **33**, 857–871, https://doi.org/10.1175/WAF-D-18-0030.1.

Vischel, T., and Coauthors, 2019: Precipitation extremes in the West African Sahel: Recent evolution and physical mechanisms. *Tropical Extremes*, V. Venugopal et al., Eds., Elsevier, 95–138.

Vizy, E. K., and K. H. Cook, 2018: Mesoscale convective systems and nocturnal rainfall over the West African Sahel: Role of the inter-tropical front. *Climate Dyn.*, **50**, 587–614, https://doi.org/10.1007/s00382-017-3628-7.

——, and ——, 2022: Distribution of extreme rainfall events and their environmental controls in the West African Sahel and Soudan. *Climate Dyn.*, **59**, 997–1026, https://doi.org/10.1007/s00382-022-06171-x.

Vogel, P., P. Knippertz, A. H. Fink, A. Schlueter, and T. Gneiting, 2018: Skill of global raw and postprocessed ensemble predictions of rainfall over northern tropical Africa. *Wea. Forecasting*, **33**, 369–388, https://doi.org/10.1175/WAF-D-17-0127.1.

——, ——, ——, ——, and ——, 2020: Skill of global raw and postprocessed ensemble predictions of rainfall in the tropics. *Wea. Forecasting*, **35**, 2367–2385, https://doi.org/10.1175/WAF-D-20-0082.1.

——, ——, T. Gneiting, A. H. Fink, M. Klar, and A. Schlueter, 2021: Statistical forecasts for the occurrence of precipitation outperform global models over northern tropical Africa. *Geophys. Res. Lett.*, **48**, e2020GL091022, https://doi.org/10.1029/2020GL091022.

Vondou, D. A., M. Maranan, A. H. Fink, and P. Knippertz, 2026: Meteorological conditions leading to a catastrophic, rain-induced landslide in Cameroon in October 2019. *Quart. J. Roy. Meteor. Soc.*, e70066, https://doi.org/10.1002/qj.70066, in press.

Walz, E.-M., M. Maranan, R. van der Linden, A. H. Fink, and P. Knippertz, 2021: An IMERG-based optimal extended probabilistic climatology (EPC) as a benchmark ensemble forecast for precipitation in the tropics and subtropics. *Wea. Forecasting*, **36**, 1561–1573, https://doi.org/10.1175/WAF-D-20-0233.1.

——, P. Knippertz, A. H. Fink, G. Köhler, and T. Gneiting, 2024: Physics-based vs data-driven 24-hour probabilistic forecasts of precipitation for northern tropical Africa. *Mon. Wea. Rev.*, **152**, 2011–2031, https://doi.org/10.1175/MWR-D-24-0005.1.

Ward, P. J., and Coauthors, 2020: The need to integrate flood and drought disaster risk reduction strategies. *Water Secur.*, **11**, 100070, https://doi.org/10.1016/j.wasec.2020.100070.

Wilheit, T. T., 1986: Some comments on passive microwave measurement of rain. *Bull. Amer. Meteor. Soc.*, **67**, 1226–1232, https://doi.org/10.1175/1520-0477(1986)067<1226:SCOPMM>2.0.CO;2.

Xu, W., H. Chen, H. Wei, Y. Luo, and T. Zhao, 2022: Extreme precipitation produced by relatively weak convective systems in the tropics and subtropics. *Geophys. Res. Lett.*, **49**, e2022GL098048, https://doi.org/10.1029/2022GL098048.

Zahiri, E., and Coauthors, 2023: 5 minutes rainfall in Abidjan district (Côte d'Ivoire) (2015-). Dataverse, accessed 27 January 2026, https://doi.org/10.23708/JOE1X6.

Zsótér, E., 2006: Recent developments in extreme weather forecasting. *ECMWF Newsletter*, No. 107, ECMWF, Reading, United Kingdom, 8–17, https://doi.org/10.21957/KL9821HNC7.